# RARE GAS CONSTRAINTS ON THE HISTORY OF BOULDER 1, STATION 2, APOLLO 17

D. A. LEICH, S. B. KAHL*, A. R. KIRSCHBAUM**,
S. NIEMEYER, and D. PHINNEY
*Dept. of Physics, University of California, Berkeley, Calif., U.S.A.*

(Received 2 September, 1975)

**Abstract.** Rare gas isotopic analyses have been performed on both pile-irradiated and unirradiated samples from Boulder 1, Station 2. Two samples from rock 72255, the Civet Cat clast and a sample of adjacent breccia, have concordant $^{40}Ar$–$^{39}Ar$ ages of $3.99 \pm 0.03$ b.y. and $4.01 \pm 0.03$ b.y., respectively. Several samples from rock 72275 have complex thermal release patterns with no datable features, but an intermediate-temperature plateau from the dark rim material of the Marble Cake clast yields an age of $3.99 \pm 0.03$ b.y. – indistinguishable from the age of rock 72255. We regard these ages as upper limits on the time of the Serenitatis basin-forming event.

The absence of fossil solar-wind trapped gases in the breccia samples implies that a prior existence for the boulder as near-surface regolith material can be regarded as extremely unlikely. Instead, the small trapped rare-gas components have isotopic and elemental compositions diagnostic of the terrestrial-type trapped component which has previously been identified in several Apollo 16 breccias and in rock 14321. Excess fission Xe is found in all Boulder 1 samples in approximately 1:1 proportions with Xe from spontaneous fission of $^{238}U$. This excess fission Xe is attributed to spontaneous fission of $^{244}Pu$ *in situ*.

Cosmic-ray exposure ages for samples from rocks 72215 and 72255 are concordant, with mean $^{81}Kr$–Kr exposure ages of $41.4 \pm 1.4$ m.y. and $44.1 \pm 3.3$ m.y., respectively. However a distinctly different $^{81}Kr$–Kr exposure age of $52.5 \pm 1.4$ m.y. is obtained for samples from rock 72275. A two-stage exposure model is developed to account for this discordance and for the remaining cosmogenic rare-gas data. The first stage was initiated at least 55 m.y. ago, probably as a result of the excavation of the boulder source-crop. A discrete change in shielding depths $\sim 35$ m.y. ago probably corresponds to the dislodgement of Boulder 1 from the South Massif and emplacement in its present position.

## 1. Introduction

We have undertaken a comprehensive study of rare gases in samples from Boulder 1, Station 2, Apollo 17. The overall objective of our Consortium Indomitabile effort has been to obtain as much information as could be extracted from rare gases in these samples so that a detailed history for Boulder 1 could be synthesized in conjunction with the other Consortium studies. To this end, we have directed our attention to three specific problems. The first is $^{40}Ar$–$^{39}Ar$ dating of Boulder 1 samples, with a well-defined bearing on the age of the Serenitatis basin. Second is the determination of the abundances and isotopic compositions of trapped rare gases and fission xenon with implications regarding the origin of the boulder. The third problem is the detailed analysis of cosmic-ray produced rare gas isotopes to discover the complete exposure history of Boulder 1. In this paper we present the experimental results and major conclusions of this intensive study of a single lunar object.

* Present address: Dept. of Chemistry, Wellesley College, Wellesley, Mass., U.S.A.
** Present address: Office of Institutional Research, University of California, Berkeley, Calif., U.S.A.

*The Moon* **14** (1975) 407–444. 

## 2. Sample Preparation and Experimental Procedure

Our analyses of Consortium Indomitabile samples include three samples from rock 72215, two from rock 72255, and six from rock 72275. Most samples were portions of collective allocations to the Anders, Haskin, and Reynolds groups, and therefore bear sample numbers which are common to the three groups. We had originally believed that these samples would be crushed and homogenized before being divided among the separate groups, as we were hoping to rely on the rather extensive chemical analyses by the Anders (Morgan *et al.*, 1975) and Haskin (Blanchard *et al.*, 1975) groups in our analyses of rare gas data (e.g., calculations involving production rates for cosmogenic rare gases from specific target elements). In each case, however, the portion analyzed by Morgan *et al.* (1975) was a single chip (or a few small chips) selected or broken from the original allocation. Thus we cannot apply the chemical data obtained from these samples to our own analyses without allowing for potentially large inhomogeneities between the corresponding samples. Our portions of samples 72255,42, 72255,52, and 72275,57 were received as large fragments, implying that the applicability of the data of Blanchard *et al.* (1975) to our analyses of these samples is also compromised by the possibility of chemical inhomogeneities. The same conclusion applies to samples 72275,80 and 72275,91 for similar reasons. The remaining six samples (samples 76, 83, and 166 from rock 72275 and all three samples from rock 72215) were each crushed and homogenized before splitting into a portion for rare gas analysis and a portion for chemical analysis. Thus chemical data from these splits can be considered as representative analyses of the corresponding rare gas samples. More detailed documentation of sample locations, descriptions, and processing have been given elsewhere (Marvin, 1974a, b; Blanchard *et al.*, 1974). We shall frequently refer to samples by the abbreviated rock names used throughout this series of Consortium Indomitabile papers: AnBx = anorthositic breccia, BCBx = black competent breccia, CN = coarse norite, GCBx = grey competent breccia, LFBx = light friable breccia, and PB = pigeonite basalt (Marvin, 1975).

The samples received for rare gas analyses were further divided into three portions. Samples including large fragments were crushed and homogenized, then portions for pile-irradiation were separated. (These are not careful splits, although some attempt was made to divide the samples with a spatula on the weighing paper.) The bulk of each of the remaining portions was then consumed in a complete rare gas analysis; however, a small (10–20 mg) aliquot of each sample was saved for additional chemical analyses.

Each sample destined for pile irradiation was placed in an evacuated quartz ampoule along with a Ni fluence-monitoring wire. Ampoules were also prepared for a Ca-monitor (optical grade $CaF_2$), a K-monitor (reagent grade $K_2SO_4$), and two age monitors (St. Severin chondrite). The samples and monitors were loaded together in one layer of an irradiation capsule designated MIDT # 1. The capsule was irradiated in the USGS TRIGA reactor at Denver, Colorado. After the irradiation the samples were removed from the ampoules, wrapped in aluminum foil, and loaded into the

extraction manifold of the mass spectrometer system designated as BMS2. The Ni fluence monitors were also removed at this time, and fluences relative to the age monitor were determined by counting the $^{58}$Co activities in the wires.

The samples were analyzed mass spectrometrically according to the procedures listed in Phinney *et al.* (1975) and references therein. The age monitors give a $J$-value for this irradiation of

$$J = 0.01361 \pm 0.00024,$$

where $J = (e^{\lambda Tm} - 1)/(^{40}*\text{Ar}/^{39}*\text{Ar})_{\text{monitor}}$, $\lambda = 5.305 \times 10^{-10}$ yr$^{-1}$, and $Tm = (4.504 \pm 0.020) \times 10^9$ yr. The K and Ca monitors gave the following conversion factors for the irradiation:

$$\frac{^{39}*\text{Ar}}{\text{K}} = (1.64 \pm 0.20) \times 10^{-4} \frac{\text{cm}^3 \text{ STP}}{\text{g}}$$

and

$$\frac{^{37}*\text{Ar}}{\text{Ca}} = (9.7 \pm 2.0) \times 10^{-5} \frac{\text{cm}^3 \text{ STP}}{\text{g}}.$$

Data reduction was performed in the manner described by Phinney *et al.* (1975). The data which appear in the Data Appendix (Table A.1) have been corrected for:

(1) Mass discrimination.

(2) The decay of $^{37}$Ar and $^{39}$Ar during and after irradiation [$\lambda_{37} = (1.974 \pm 0.0056) \times 10^{-2}$ day$^{-1}$ and $\lambda_{39} = (7.05 \pm 0.079) \times 10^{-6}$ day$^{-1}$].

(3) Blanks (typical $^{40}\text{Ar}_{\text{blank}} \sim 1 \times 10^{-8}$ cm$^3$ STP).

(4) Reactor-derived Ca-interferences for $^{36}$Ar, $^{38}$Ar, and $^{39}$Ar [$^{36}\text{Ar}/^{37}\text{Ar} = (2.724 \pm 0.08) \times 10^{-4}$, $^{38}\text{Ar}/^{37}\text{Ar} = (3.17 \pm 0.02) \times 10^{-5}$, and $^{39}\text{Ar}/^{37}\text{Ar} = (6.785 \pm 0.026) \times 10^{-4}$].

(5) Reactor-derived K-interferences for $^{38}$Ar and $^{40}$Ar [$^{38}\text{Ar}/^{39}\text{Ar} = (1.340 \pm 0.0024) \times 10^{-2}$ and $^{40}\text{Ar}/^{39}\text{Ar} = 0.001 \pm 0.001$].

(6) Mass spectrometer sensitivity variations.

Experimental uncertainties have been compounded quadratically at each step in the data reduction procedure.

Neutron fluences as deduced from the Ni fluence monitors showed a flux gradient of 4% per cm along the long axis of the sample ampoules. However, the ampoules received total neutron doses which were within $\pm 1\%$ of that received by the age monitors. Although the analytical precision of the relative fluence measurements is $\pm 0.6\%$, we prefer a more conservative estimate of $\pm 1\%$ for these fluences, which corresponds to $\sim \pm 0.02$ b.y. uncertainties in the *relative* gas-retention ages for the samples in this irradiation.

Table I summarizes the plateau ages, total $^{40}\text{Ar}/^{39}\text{Ar}$ ages, $^{38}$Ar–Ca exposure ages, K-contents, and Ca-contents for our samples. These quantities were calculated from the data in Table A.1 according to the procedures in Alexander and Kahl (1974).

TABLE I

Plateau ages, total $^{40}Ar$–$^{39}Ar$ ages, $^{38}Ar$–Ca exposure ages and elemental abundances for pile-irradiated samples

| Sample | 72255 | | 72275 | | | | |
|---|---|---|---|---|---|---|---|
| | ,42 | ,52 | ,57 | ,76 | ,80 | ,83 | ,91 |
| Plateau age (b.y.) | 3.99±0.03 | 4.01±0.03 | – | – | 3.99±0.03 | – | – |
| Total $^{40}Ar$–$^{39}Ar$ age (b.y.) | 3.96±0.03 | 3.89±0.03 | 3.68±0.03 | 3.73±0.03 | 3.89±0.03 | 3.97±0.03 | 3.63±0.03 |
| $^{38}Ar$–Ca exposure age (m.y.)[a] | 48 | 56 | 75 | 71 | 75 | 75 | 75 |
| K (wt. %)[b] | 0.14 | 0.23 | 0.25 | 0.33 | 0.34 | 0.23 | 0.24 |
| Ca (wt. %)[c] | 9.3 | 8.6 | 8.4 | 10.4 | 6.1 | 8.5 | 8.3 |
| Br[d] | 1.05 | – | – | – | 5.4 | – | ≡1 |
| I[d] | 0.60 | – | – | – | 0.64 | – | ≡1 |
| Ba[d] | 0.69 | – | – | – | 2.2 | – | ≡1 |
| U[d] | 0.60 | – | – | – | 2.2 | – | ≡1 |

[a] Error estimated to be 25%.
[b] Error estimated to be 15%.
[c] Error estimated to be 25%.
[d] Amounts normalized to that in 72275,91; errors in Br, I, and Ba estimated to be 15%; error in U estimated to be 33%.

For three samples (72255,42, 72275,80, and 72275,91) we also analyzed Kr and Xe in order to measure relative Br, I, Ba, and U concentrations. These concentrations were deduced according to the procedures of Alexander and Davis (1974) and appear also in Table I.

In our first Consortium report (Leich *et al.*, 1974) we made note of a calibration problem in the absolute gas abundances calculated for the BMS2 system. We have subsequently analyzed an aliquot of the Berkeley Bruderheim standard and have obtained good agreement with the 'world average' gas concentrations for this standard. However, we are still not satisfied with the BMS2 gas concentration data since conventional K–Ar ages calculated from these data are systematically high compared to the total $^{40}Ar/^{39}Ar$ ages, and since the $^{38}Ar$–Ca exposure ages for the pile-irradiated samples are systematically high compared to $^{38}Ar$ exposure ages measured in aliquots on the BMS4 system (see below). As has been previously pointed out, our $^{40}Ar$–$^{39}Ar$ gas-retention ages, K-contents, Ca-contents, and the other relative elemental contents are independent of absolute gas concentrations and are not subject to this problem.

The sample portions designated for rare gas analyses were processed in a separate extraction-manifold and mass-spectrometer system (designated BMS4), according to procedures similar to those described by Hohenberg *et al.* (1970) and Srinivasan (1973). Most samples were subjected to a two-step temperature extraction program (600 °C and 1650 °C for 72255 and 72275 samples; 700 °C and 1650 °C for 72215 samples); however, an additional temperature step (1100 °C) was included for two samples (72275,57 and 72275,166), and a single temperature extraction (1650 °C) was used for one small sample (72275,91). All samples melted in the 1650 °C heating. Extracted gases were separated into He–Ne, Ar, Kr and Xe fractions for sequential

TABLE II

Sr, Zr, Ba, and U abundances (ppm) [a]

| Sample | Sr | Zr | Ba | U |
|---|---|---|---|---|
| 72255,42 (CN) | 139 | 132 | 172 | 0.45 |
| 72255,52 (GCBx) | 140 | 376 | 324 | 1.42 |
| 72275,57 (LFBx) | 112 | 667 | 346 | 1.52 |
| 72275,76 (AnBx) | 171 | 479 | 361 | 1.60 |
| 72275,80 (BCBx) | 151 | 908 | 683 | 3.19 |
| 72275,91 (PB) | 92 | 625 | 355 | 1.53 |

[a] Data are from aliquots analyzed by B. M. Bansal and H. Wiesmann. Uncertainties are estimated to be better than ±5%.

analysis in the mass spectrometer. Blank corrections were applied to the resulting data, compounding uncertainties with uncertainties ($1\sigma$) in the measured compositions. The resulting rare gas isotopic analyses of Boulder 1 samples are given in the Data Appendix (Tables A.2–A.4). The sometimes quite large uncertainties in $^{20}Ne/^{22}Ne$ ratios in Table A.2 are due to the substantial corrections applied to $^{20}Ne$ for $^{40}Ar^{++}$. Interference with hydrocarbon background contamination in Kr (Table A.3) and Xe (Table A.4) was negligible.

Chemical analyses of the small remaining portions of our Boulder 1 samples are still incomplete, but first results are given in Table II. These analyses were performed for us by B. M. Bansal and H. Wiesmann using isotope dilution techniques described by Gast *et al.* (1970). More complete chemical data will be forthcoming (N. J. Hubbard, private communication).

## 3. $^{40}Ar$–$^{39}Ar$ Dating

The interpretation of $^{40}Ar$–$^{39}Ar$ data for 'whole-rock' samples of lunar breccias requires considerable care (see e.g. Jessberger *et al.*, 1974). It is therefore worthwhile to review the criteria we have used for extracting chronological information from our samples of Boulder 1.

The cardinal requirement is a plateau in an apparent-age plot (see e.g. Figure 1). A plateau, as we use the term, consists of *at least* three consecutive temperature fractions with $^{40}*Ar/^{39}*Ar$† ratios whose $\pm 2\sigma$ uncertainty intervals overlap the $^{40}*Ar/^{39}*Ar$ ratio of the plateau. The $^{40}*Ar/^{39}*Ar$ ratio of the plateau is the weighted (by $^{39}*Ar$) mean of $^{40}*Ar/^{39}*Ar$ ratios for the temperature fractions on the plateau.

For breccias, such as Boulder 1, the plateau age is usually interpreted as the time of the last major metamorphic event in the history of the rock. However, the confidence with which one treats such a plateau age as significant is conditioned by the following considerations:

(1) The fraction of the total $^{39}*Ar$ which is released in the plateau temperature steps. Clearly, the greater this fraction the less likely it is that the plateau is an experimental artifact or coincidence.

(2) The K/Ca ratios for the plateau steps. The K/Ca ratio is often useful for discerning different mineral phases which outgas in different temperature steps. Moreover, relatively constant K/Ca ratios in conjunction with an apparent-age plateau usually imply gas release from a chemically homogeneous mineral system which should yield a well-defined age (Turner *et al.*, 1972).

(3) The $^{38}Ar_c/^{37}Ar$ for the plateau steps. The $^{38}Ar_c/^{37}Ar$ ratio is dependent on the relative concentrations of the spallation target elements, Ca, Fe, and Ti. As with K/Ca ratios, a substantially constant $^{38}Ar_c/^{37}Ar$ is indicative of outgassing from a chemically homogeneous mineral system.

† In this paper we use the following customary notation. An asterisk (*) in connection with $^{40}Ar$ and $^{39}Ar$ indicates that the isotope is potassium-derived. The subscript '*c*' is used to identify cosmogenic (cosmic-ray derived) components.

(4) The amount of nonradiogenic $^{40}Ar$. To calculate a plateau age, the amount of $^{40}Ar$ in a temperature step must be partitioned into a radiogenic fraction and a nonradiogenic (i.e., trapped and spallation) fraction. All other things being equal, the partitioning process introduces some additional uncertainty in the plateau age. The most reliable ages are thus those from samples with a negligible proportion of nonradiogenic $^{40}Ar$.

(5) Concordance with ages of the same sample using other dating techniques.

(6) Agreement with ages obtained for other samples which have been collected from the same locality as the sample in question and/or which show petrological and compositional evidence for a contemporaneous origin.

In connection with samples from Boulder 1, one factor which can be dispensed with immediately is that of nonradiogemic $^{40}Ar$. The ratio of nonradiogenic $^{40}Ar$ to total $^{40}Ar$ is less than 0.1% for all of our samples. There is preferential release of nonradiogenic $^{40}Ar$ in some temperature steps of 72255,52 (700, 800 °C), 72275,80 (800, 900 °C), and 72275,91 (1100, 1200, 1400 °C); but in these cases the amounts are still $\leqslant 0.17\%$ of the $^{40}*Ar$. This has no observable effect on the precision of the $^{40}*Ar/^{39}*Ar$ ratios.

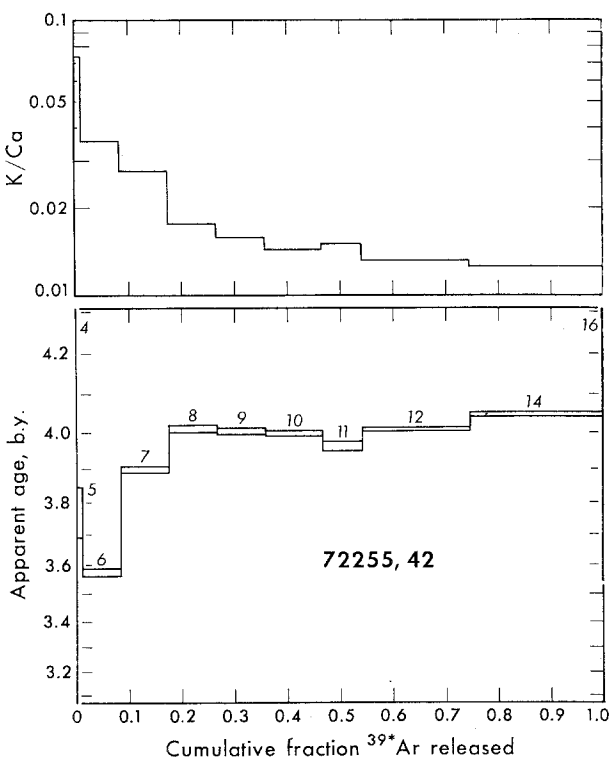


Fig. 1. Apparent-age and K/Ca data from 72255,42. In this and Figures 2–5 the numbers by the data values are the temperature of the fraction in hundreds of degrees C. The plateau (800–1200 °C) gives an age of $3.99 \pm 0.03$ b.y. for this sample.

### 3.1. 72255

Figure 1 shows the apparent-age plot and K/Ca ratios for 72255,42, the Civet Cat clast. The first four temperature fractions (400–700 °C) show evidence of $^{40}$*Ar loss and have K/Ca ratios which are high relative to the later temperature fractions. From 800 °C through 1200 °C this sample has an apparent-age plateau which corresponds to an age of 3.99 ± 0.03 b.y. The plateau includes 57% of the total $^{39}$*Ar. The 1400 °C fraction, which contains 25% of the total $^{39}$*Ar, has a $^{40}$*Ar/$^{39}$*Ar significantly higher than the plateau value.

The K/Ca ratio in the plateau fractions decreases slightly, amounting to ~30% relative to the mean value. The $^{38}Ar_c/^{37}Ar$ ratio is virtually constant for all temperature fractions above 700 °C. Thus the Ar isotopic data, considered as a whole, suggest that the plateau age should be reliable.

Compston *et al.* (1975) have presented Rb–Sr evidence for a 4.17 ± 0.05 b.y. igneous age for the Civet Cat clast. However, certain mineral fractions from this clast show signs of a later disturbance of the Rb–Sr system. Compston *et al.* (1975) calculate a

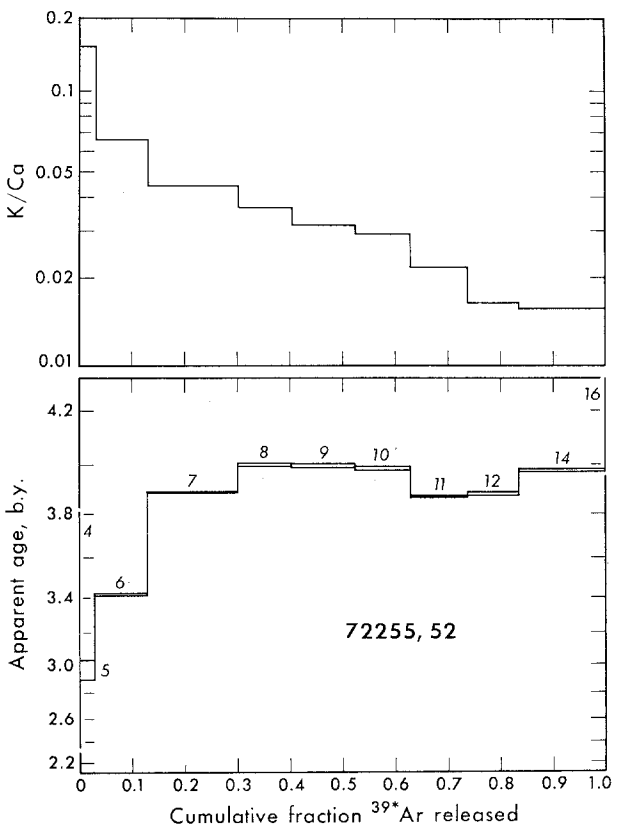


Fig. 2. Apparent-age and K/Ca data from 72255,52. The intermediate-temperature (800–1000 °C) plateau corresponds to an age of 4.01 ± 0.03 b.y.

model age for the disturbance of 3.9±0.1 b.y., a result which is consistent with the $^{40}Ar$–$^{39}Ar$ plateau age.

The higher $^{40}Ar$–$^{39}Ar$ apparent age in the 1400°C fraction of our sample may reflect the presence of minerals whose argon clocks were not reset in the 3.99 b.y. event. The Rb–Sr work of Compston *et al.* (1975) has established the presence of material older than 3.99 b.y. in the Civet Cat clast. Furthermore, Jessberger *et al.* (1974) have seen evidence, in a high resolution outgassing sequence of plagioclase from 65015, for a high-temperature increase in $^{40}Ar$–$^{39}Ar$ apparent age which they attribute to older, relict grains in their sample. We suspect therefore that the apparent-age increase in the 1400°C fraction is due to this effect, although a high-resolution outgassing sequence such as employed by Jessberger *et al.* (1974) will be necessary to establish this result in a quantitative way.

Figure 2 contains the apparent-age and K/Ca plots for a sample of matrix material (72255,52) adjacent to the Civet Cat clast. For this sample the initial temperature fractions, which indicate $^{40}*Ar$ loss, are followed by an intermediate-temperature (800–1000°C) plateau with an apparent age of 4.01 ± 0.03 b.y. There is a drop-off in

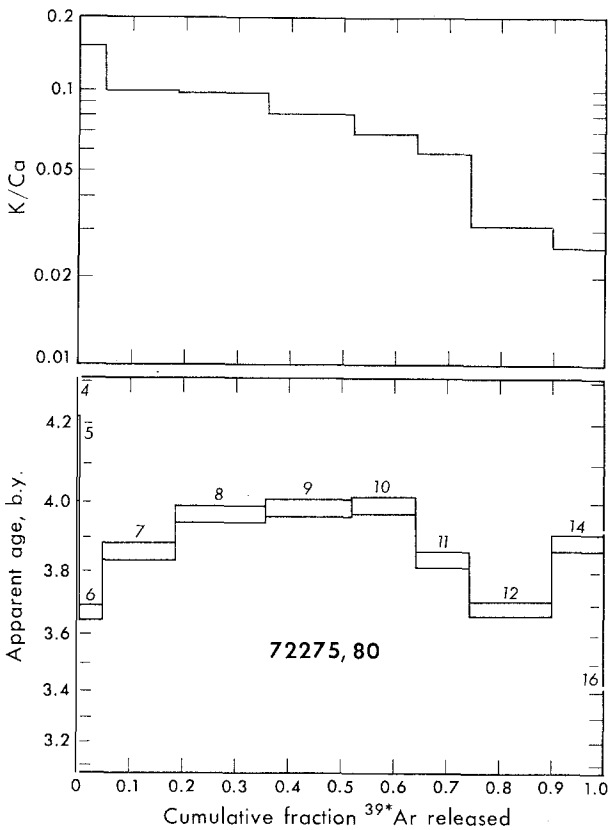


Fig. 3. Apparent-age and K/Ca data from 72275,80. The intermediate-temperature (800–1000°C) plateau gives an age of 3.99±0.03 b.y.

apparent age for the 1100 and 1200 °C fractions, with a recovery to the plateau value in the 1400 °C fraction.

The K/Ca ratio decreases by ~25% over the plateau with steeper changes for temperature fractions before and after the plateau. As with 72255,42, the $^{38}Ar_c/^{37}Ar$ is relatively constant for all temperature fractions above 700 °C.

Although only 33% of the total $^{39}$*Ar in this sample is released in the plateau steps, there is justification for treating the plateau age as reliable. The primary reason is the agreement of the plateau age with that of the adjacent Civet Cat clast. Secondarily, we note that many studies (see, e.g., Turner *et al.*, 1973; Huneke *et al.*, 1973) have shown that intermediate-temperature plateaux for 'whole-rock' samples can yield realistic and accurate gas-retention ages. We thus have a mean $^{40}Ar$–$^{39}Ar$ age for our two samples of 72255 of 4.00±0.03 b.y. and feel that this age is an accurate measurement of the time that 72255 began retention of argon.

### 3.2. 72275

We have analyzed five samples of 72275 with the $^{40}Ar$–$^{39}Ar$ technique, but only one

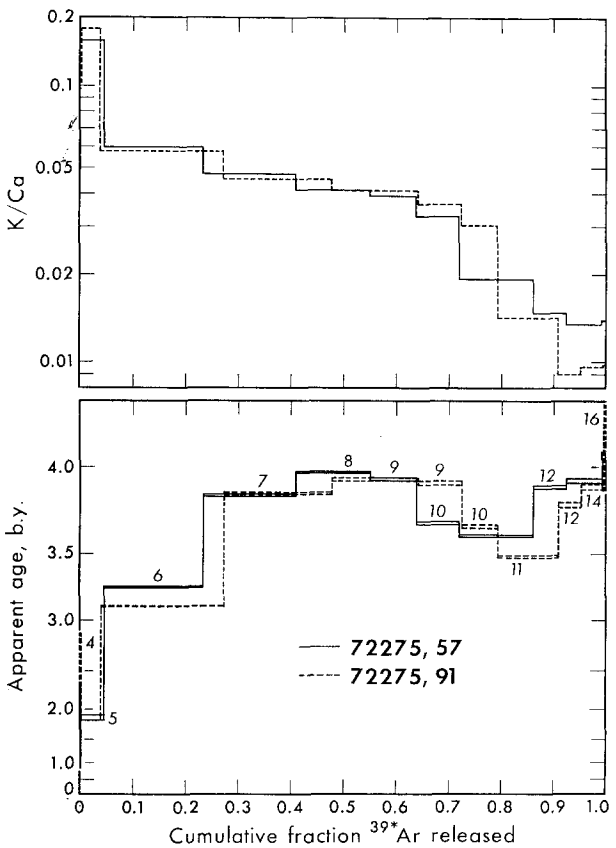


Fig. 4. Apparent-age and K/Ca data from 72275,57 and 72275,91.

sample has proved to be datable. Figure 3 shows the apparent-age and K/Ca plots for this sample, 72275,80. The apparent-age pattern is quite similar to that for 72255, 52. The intermediate-temperature plateau has an apparent age of $3.99 \pm 0.04$ b.y.

This plateau includes 46% of the total $^{39}$*Ar released from the sample. The K/Ca ratio drops uniformly by ~36% throughout the plateau steps. There is a sharp increase in $^{38}Ar_c/^{37}Ar$ in the 1000 °C step, which is not paralleled by a sharp change in K/Ca, apparent age, or $^{37}$Ar content. This behavior means that there is an excess of $^{38}Ar_c$ which is uncorrelated with $^{37}$Ar (i.e., uncorrelated with Ca), and we believe that it signals the onset of outgassing from a mineral rich in Fe and/or Ti, the other two primary target elements for $^{38}Ar_c$. We would expect such behavior to cut short the intermediate-temperature plateau. However, the plateau is clear-cut, and the age is in excellent agreement with the mean $^{40}$Ar–$^{39}$Ar age of 72255.

The apparent-age and K/Ca plots for the other 72275 samples are shown in Figures 4 and 5. Unlike 72275,80, the incipient apparent-age plateaux for these samples are all cut short by a drop-off in the 1000 °C fractions. The drop-off is in all cases accompanied by a sharply increased $^{38}Ar_c/^{37}Ar$ ratio (as much as a factor of two for 72275,57) beginning in the 900 °C fractions. The K/Ca ratios usually show

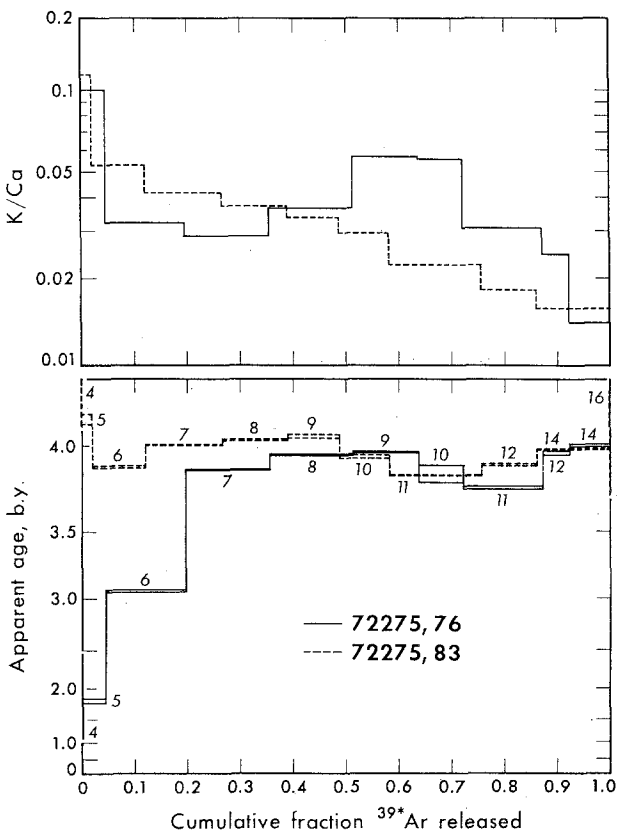


Fig. 5. Apparent-age and K/Ca data from 72275,76 and 72275,83.

the greatest change at 1100 °C. It appears then that outgassing from Fe- and/or Ti-bearing materials has truncated the plateaux to only two temperature steps, and thus the data are not adequate for chronological interpretation.

### 3.3. Chronological implications

There is now firm evidence that Boulder 1 was assembled during the interval from ~4.0 to ~3.9 b.y. ago. The lower limit is set by the age of the oldest basalt from the Taurus-Littrow region, since the boulder does not contain any mare basalt fragments (Ryder *et al.*, 1975). The oldest mare basalt yet reported for Apollo 17 samples is 78503, whose age is 3.89±0.03 b.y. (Schaeffer and Husain, 1975). The upper limit is set by the youngest *igneous* ages for clasts in the boulder breccias. In the competent breccias (GCBx and BCBx) the youngest age is found in microgranite clasts from 72215 and 72255 (Rb–Sr age = 4.03±0.03 b.y.; Compston *et al.*, 1975). The youngest igneous age in the LFBx is found in a pigeonite basalt clast from 72275 (Rb–Sr age = 4.01±0.04 b.y.; Compston *et al.*, 1975). Our $^{40}Ar$–$^{39}Ar$ plateau ages fall within these limits and probably date an event in the consolidation of the boulder.

For several reasons the material of the boulder is thought to have experienced at least two heating episodes during the above interval. Petrographic investigations (Ryder *et al.*, 1975) indicate that the earlier episode took place at temperatures high enough to melt granite ($T > 990$ °C) and involved the formation and compaction of the GCBx and BCBx materials. The later episode occurred at distinctly cooler temperatures and is associated with the formation of the LFBx material. Ryder *et al.* (1975) have conjectured that this second event may have emplaced the boulder in the South Massif.

Natural remanent magnetism (NRM) studies (Banerjee and Swits, 1975) also point to two thermal episodes in the boulder's history. The earlier, higher-temperature event is documented by widely divergent directions of stable NRM components in 72215, 72255, and 72275. The second event is characterized by coincident directions of less stable magnetization which appear to have been imprinted on the rocks at a temperature of ~450°.

The $^{40}Ar$–$^{39}Ar$ ages probably date the earlier of these two events, i.e. the formation of the GCBx and BCBx. We note first that the ages of the GCBx from 72255 and of the BCBx from 72275 are in excellent agreement and have a mean of 4.00±0.03 b.y. Second, the plateau age of the Civet Cat clast, which is embedded in GCBx, also agrees with the GCBx and BCBx mean age. These ages are thus consistent with a single event (within the ±20 m.y. resolution of our method). Moreover, the event was sufficiently intense to reset the K–Ar clock of the Civet Cat clast, which is known from Rb–Sr dating (Compston *et al.*, 1975) to have existed for at least ~170 m.y. prior to the event 4.00 b.y. ago.

It is, of course, possible that the K–Ar clock was reset in the first event and then reset again in the later cooler event. We are inclined to discount this possibility, since the temperature (~450 °C) deduced from the NRM measurements was probably too low to outgas $^{40}*Ar$ quantitatively.

The last chronological consideration is the relationship of the $^{40}Ar$–$^{39}Ar$ ages for Boulder 1 samples to the age of the Serenitatis basin-forming event. The most critical constraints on this relationship appear to us to be the following:

(1) The boulder was once a 'clast' buried in the South Massif. Photogeological evidence (Wolfe, 1975) points to a Serenitatis origin for the South Massif. Wolfe further concludes that contributions from post-Serenitatis basins, if present, are insignificant. This constraint, taken at face value, implies that the $^{40}Ar$–$^{39}Ar$ ages of the boulder cannot be younger than the age of Serenitatis.

(2) The boulder contains a meteoritic component (Group 3 of Morgan *et al.*, 1975) which is distinct from the meteoritic component (Group 2) in essentially all of the other Apollo 17 breccias which have been studied. Morgan *et al.* (1975) have concluded that the Group 2 meteoritic component must be associated with the Serenitatis projectile. For several reasons they have argued that the Group 3 component in the boulder is pre-Serenitatis. This constraint therefore allows for the possibility that the $^{40}Ar$–$^{39}Ar$ ages are pre-Serenitatis.

These two constraints can be accommodated in a single model for the origin of Boulder 1: namely, the GCBx (and BCBx) materials were formed in an impact of the Group 3 projectile. This impact would be the high temperature event discussed above and is the one documented by the mean $^{40}Ar$–$^{39}Ar$ age of $4.00 \pm 0.03$ b.y. The cooler event is identified with the Serenitatis impact and, following the lead of Ryder *et al.* (1975), would be responsible for both the assembly of the LFBx in the boulder and the boulder's emplacement in the South Massif.

This model is by no means unique. A number of other possible models are explored in the papers in this issue. However, all models must reckon with the constraints listed above, and, in our estimation, these constraints require that 4.00 b.y. be considered as a firm upper limit on the age of the Serenitatis basin-forming event.

## 4. Trapped Rare Gases and Fission Xenon

The rare gas contents of unirradiated samples from Boulder 1 can be separated into four distinct components: cosmogenic, radiogenic, fissiogenic, and trapped. A detailed discussion of the cosmogenic component, which includes rare gas isotopes produced by cosmic-ray induced spallation reactions as well as reactions with secondary particles, will be given in the next section. The observed $^{40}Ar$ abundances are almost purely radiogenic and allow calculation of K–Ar ages ranging from 3.7–4.3 b.y. for most samples, using K determinations from Blanchard *et al.* (1974). The chronological significance of these ages does not compare with the much more precise $^{40}Ar$–$^{39}Ar$ ages; they do, however, provide a useful check on the accuracy of measured $^{40}Ar$ abundances and on the applicability of the chemical analyses by Blanchard *et al.* (1974) to the samples used for rare gas measurements. The 3.7–4.3 b.y. range of K–Ar ages is in fairly good agreement with the 4.0 b.y. $^{40}Ar$–$^{39}Ar$ age, considering the uncertainties in the $^{40}Ar$ abundance measurements. Two exceptions are the Civet Cat sample (72255,42) and one of the BCBx samples (72275,80) from the Marble Cake

clast. We calculate unreasonably high K–Ar ages of 5.0 b.y. and 4.5 b.y., respectively, for these two samples. This discrepancy is remedied for Civet Cat by using the K concentration from Table I, (K–Ar age = 3.8 b.y.), leaving only 72275,80 with an unreasonable K–Ar age determination. We have interpreted this and other evidence (Leich *et al.*, 1974) as indicating gross sampling inhomogeneities in the 72255,42 Civet Cat samples distributed in the form of large chips to the Anders, Haskin, and Reynolds groups. The chemistry of the chip allocated to Reynolds should be much better represented by the data in Tables I and II since these data were obtained on splits from the crushed sample. The discrepancy for 72275,80, however, is probably due to an unreliable $^{40}$Ar determination, since the K content given in Table I is not greatly different from the value reported by Blanchard *et al.* (1974).

Besides $^{40}$Ar ,the radiogenic component also includes $^{4}$He from $\alpha$-decay of U and Th. The measured $^{4}$He/$^{20}$Ne ratios ($\sim 10^4$) are two orders of magnitude higher than in typical Apollo 17 soils and soil breccias (e.g. Hintenberger *et al.*, 1974). This clearly demonstrates that virtually all of the observed $^{4}$He in these samples is radiogenic, since a trapped solar wind component can account for only a negligible fraction ($\leqslant 1\%$) of the $^{4}$He. Using U data from Table II, Th data from Blanchard *et al.* (1974), and $^{232}$Th/$^{238}$U ratios from Nunes and Tatsumoto (1974, 1975), we calculate He–U–Th ages ranging from 2.5–3.3 b.y. Loss of 25–50% of the radiogenic He is implied for samples with a 4.0 b.y. $^{40}$Ar–$^{39}$Ar age.

Partitioning of the non-radiogenic He, Ne, and Ar between cosmogenic and trapped components is accomplished assuming isotopic compositions of trapped Ne and Ar similar to the values measured for trapped solar-wind Ne and Ar in lunar soils (see, e.g., Eberhardt *et al.*, 1972) and assuming cosmogenic ratios of $^{20}$Ne/$^{22}$Ne$\simeq$0.8, $^{21}$Ne/$^{22}$Ne$\simeq$0.9, and $^{36}$Ar/$^{38}$Ar$\simeq$0.6. The observed $^{3}$He and $^{21}$Ne abundances are almost entirely cosmogenic. Only two samples show prominent trapped Ne components: the 72275,80 Marble Cake BCBx sample and the 72255,52 GCBx sample. Figure 6 shows that these same samples also have the highest trapped Ar contents; however, all other samples have trapped Ar at the level of $\sim 10^{-8}$ cm$^3$ STP $^{36}$Ar g$^{-1}$. These trapped Ar abundances and the upper limits to trapped Ne contents are lower than the trapped gas contents of typical soils and soil breccias by four or five orders of magnitude, clearly indicating that Boulder 1 is not composed of consolidated regolith material. In fact, the 'average' breccia samples from rocks 72215 (GCBx) and 72275 (LFBx) contain trapped gases in concentrations less than or about equal to the abundances in discrete clasts with igneous lithologies (CN and PB). This strongly supports Wood's (1975) conclusion that the components of the boulder were disaggregated and reconsolidated in a single event, as even highly metamorphosed regolith material appears to be absent from these breccia samples.

The somewhat higher trapped Ne and Ar contents of the 72255,52 GCBx and the 72275,80 Marble Cake BCBx samples may well be due to a small amount of solar-wind contamination. This possibility seems especially likely for 72275,80, for which documentation (Marvin, 1974a) indicates a very shallow sampling depth, perhaps even including an exposed exterior surface of the Marble Cake rim. The fact that a

second sample of BCBx from Marble Cake (72275,166) has only one tenth the trapped Ar and less than one percent of the trapped Ne contents measured in 72275,80 supports the likelihood of a small amount of solar-wind contamination in this sample.

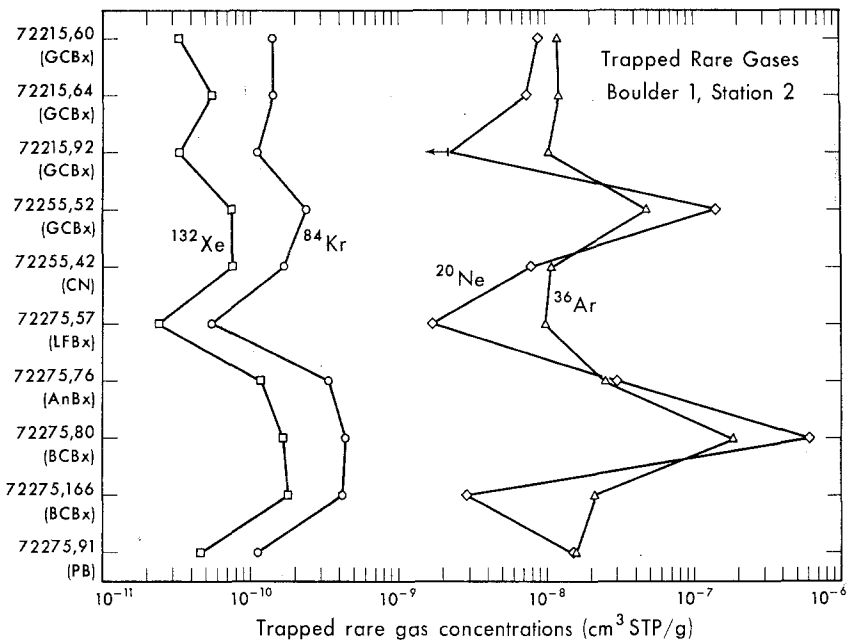


Fig. 6. Abundance of trapped $^{20}Ne$, $^{36}Ar$, $^{84}Kr$, and $^{132}Xe$ in samples from Boulder 1, Station 2.

Trapped Kr abundances are derived by first adjusting the $^{86}Kr$ yields for a small contribution from spontaneous fission of $^{238}U$ and assuming that the remainder is a mixture of trapped (BEOC 12: Eberhardt *et al.*, 1972) and cosmogenic components with $(^{86}Kr/^{83}Kr)_c \equiv 0.015 \pm 0.015$ (Marti and Lugmair, 1971). Decomposition of Xe, however, is considerably more complex, since the fissiogenic component is a major contributor to the heavy Xe isotopes and since there is a considerable difference in isotopic composition between the possible trapped components. Previous studies of cosmic-ray produced Xe have concluded that the terrestrial atmospheric composition (Nier, 1950) is a more reasonable choice for the trapped component than 'solar' Xe in many lunar rocks, because (i) Xe extracted at low temperatures (a few hundred °C) has been observed to have a terrestrial-like composition (a fact that has been generally attributed to atmospheric contamination), (ii) trapped $^{132}Xe/^{36}Ar$ ratios in most lunar rocks are considerably higher than the 'solar' ratios measured in lunar soils, (iii) the isotopic spectra of cosmogenic Xe calculated from total extractions show considerably less scatter if the trapped Xe is assumed to be terrestrial rather than solar (see, e.g., Bogard *et al.*, 1971). Recent studies of trapped Xe in lunar rocks (Lightner and Marti, 1974; Leich and Niemeyer, 1975) have shown conclusively that

the isotopic composition of trapped Xe released even at temperatures in excess of 900 °C has a terrestrial-like composition. The question of a possible lunar origin for this trapped Xe component is an important one, but has no bearing on the conclusion that the terrestrial Xe isotopic composition must be considered seriously for the trapped Xe component even in the high-temperature extractions of the present study. The isotope correlation plot shown in Figure 7 shows that the Xe from the low-temperature extractions (600 °C for 72255 and 72275 samples and 700 °C for 72215 samples) is indeed dominated by a terrestrial-like trapped component (AIR). The high-temperature (>600° or >700°) points define a linear correlation, indicating a relatively constant cosmogenic $^{128}Xe/^{126}Xe$ ratio, but the precision of the linear correlation is not sufficient to determine whether or not the trapped composition varies with increasing temperature toward a solar-type composition like SUCOR (Podosek *et al.*, 1971).

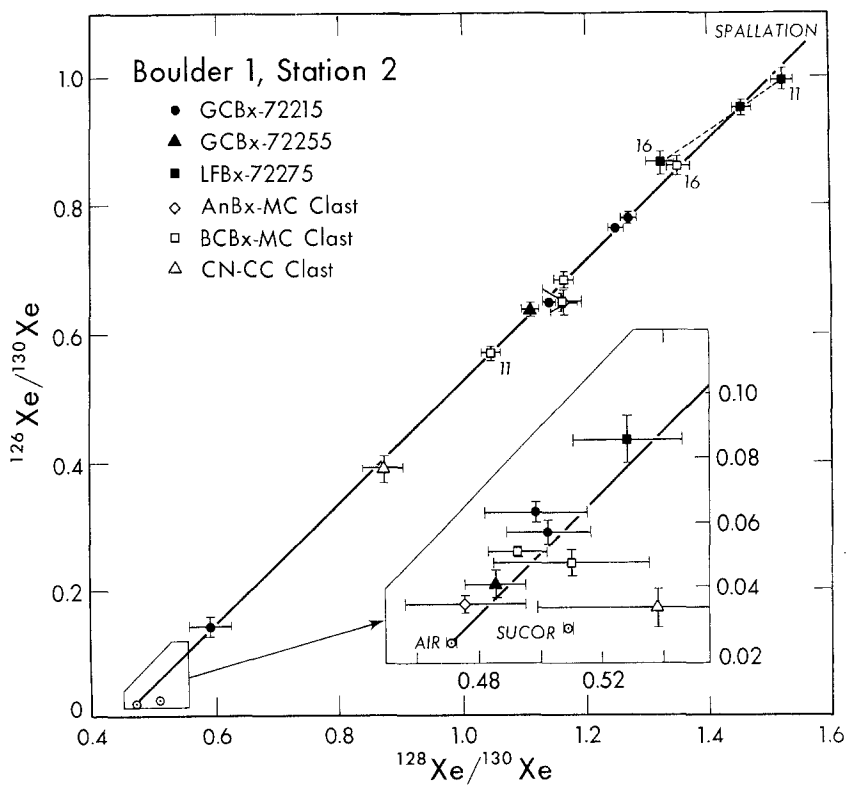


Fig. 7. Isotopic correlation of $^{126}Xe/^{130}Xe$ with $^{128}Xe/^{130}Xe$. There are at least two points corresponding to each sample. Low-temperature (600 or 700 °C) points plot in or near the insert, and are dominated by a trapped component more similar to AIR (Nier, 1950) than to SUCOR (Podosek *et al.*, 1971). High-temperature points (1650 or 1100+1650 °C) are rich in Xe from spallation. Numerical labels indicate extraction temperatures (11 for 1100 and 16 for 1650 °C) for individual data points from two samples where a three-step extraction was used (see text). The solid line is a visual fit to the data constrained to pass through the AIR point. The dashed line connects high-temperature points from LFBx sample 72275,57 showing evidence for a variable isotopic composition for Xe from spallation.

Nevertheless, we find no evidence to suggest a mixture of terrestrial and solar trapped components, as the data can be fit quite well by a mixture of a single trapped component (terrestrial) with a cosmogenic component.

In order to further evaluate the isotopic compositions of the trapped and cosmogenic components, it is necessary to consider the heavy Xe isotopes, which also include a fissiogenic component. In Figure 8 we plot $^{136}Xe/^{130}Xe$ vs $^{129}Xe/^{130}Xe$. Ideally, this set of isotopes represents a three-component mix. In the absence of a fissiogenic

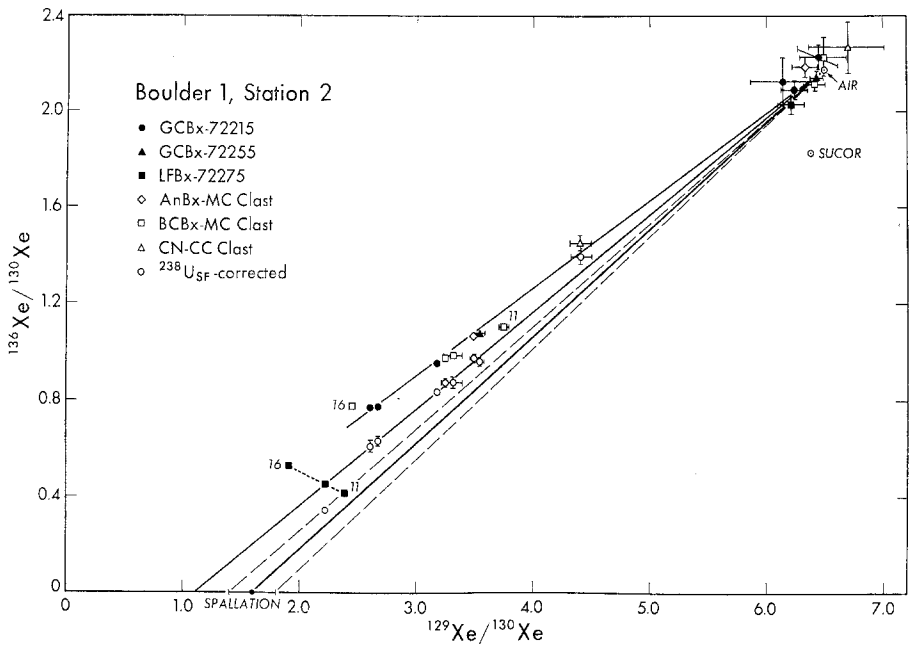


Fig. 8. Isotopic correlation of $^{136}Xe/^{130}Xe$ with $^{129}Xe/^{130}Xe$. See Figure 7 caption for explanation of data points. Open circles have been corrected for Xe from spontaneous fission of $^{238}U$ for 4.0 b.y. Subtraction of an additional fissiogenic Xe component is required, since unreasonably low yields of $^{129}Xe$ from spallation are otherwise implied. Solid lines are visual fits constrained to pass through the AIR point. The solid line flanked by long-dashed lines represents a two component mixture of trapped Xe (AIR) and Xe from spallation with $^{136}Xe/^{130}Xe \simeq 0.003$ and $^{129}Xe/^{130}Xe = 1.6 \pm 0.2$. The presence of fissiogenic $^{136}Xe$ is indicated by a vertical displacement from such a two component mixing line.

component, the data should fall on a line with end points defined by the cosmogenic and trapped compositions. The addition of fissiogenic Xe results in a vertical displacement from such a line since the fissiogenic $^{129}Xe$ and $^{130}Xe$ yields are essentially zero. The low-temperature points in Figure 8 plot near the AIR point, once again indicating that these temperature extractions are dominated by a terrestrial-like trapped component. For the high-temperature points, both 'raw' data and data from which the contribution from spontaneous fission of $^{238}U$ has been subtracted are shown. We note the rather remarkable fact that, despite the presence of three isotopically distinct components, the 'raw' high-temperature data for the GCBx, AnBx, and BCBx

samples form a rather well-defined linear array. (The point corresponding to the sum of the 1100° and 1650° extractions for BCBx sample 72275,166 is included in this linear trend even though the individual temperature points fall well off the line.) Subtraction of the $^{238}U$ spontaneous fission component preserves the linear correlation; however, an unrealistic cosmogenic $^{129}Xe/^{130}Xe$ ratio of 1.1 is implied if no additional fissiogenic Xe is present. By now, the effects of spontaneous fissioning of $^{244}Pu$ *in situ* in meteorites and old lunar rocks are documented well enough to allow us to expect comparable amounts of fissiogenic Xe from $^{244}Pu$ and $^{238}U$ in 4.0 b.y.-old lunar rocks (Podosek, 1972; Marti *et al.*, 1973a; Hutcheon and Price, 1972). Consequently we identify the additional fissiogenic Xe implied by correlation plots such as Figure 8 with this source. Using an estimate of 1.6 for the cosmogenic $^{129}Xe/^{130}Xe$ ratio and taking the trapped component to have a terrestrial composition, we conclude that the amounts of fissiogenic $^{136}Xe$ present are approximately twice the calculated contributions from $^{238}U$ for all samples except the CN and LFBx. The relatively constant ratio of $^{136}Xe$ from $^{244}Pu$ ($^{136}Xe_{PF}$) to $^{136}Xe$ from $^{238}U$ ($^{136}Xe_{UF}$) implied by this analysis validates the identification of the excess fission component with production *in situ*, and also confirms the choice of the terrestrial composition for the trapped component in the high temperature points. The correlation of the total amount of fissiogenic $^{136}Xe$ with the U content also provides the key to the linear correlation of the AnBx, BCBx, and GCBx high temperature data. Since the abundances of target elements for spallation also correlate well with U for these samples (compare Ba and U data from Table II), the cosmogenic and fissiogenic components are mixed in constant proportions. Consequently the data in Figure 8 effectively represent a two-component mix between cosmogenic-plus-fissiogenic on the one hand and trapped on the other hand. Thus the linear correlation is not fortuitous, and its extrapolation back to a trapped component much closer to the AIR composition than to SUCOR must be regarded as confirmation of a terrestrial-like trapped component in the high-temperature (>700°C) extractions from these samples. An estimate of 1.0 for the $^{136}Xe_{PF}/^{136}Xe_{UF}$ ratio is ~30% lower than would be expected from the initial $^{244}Pu/^{238}U$ ratio of 0.0154 for the St. Severin meteorite (Podosek, 1972) and the 0.50 b.y. difference in $^{40}Ar$–$^{39}Ar$ ages (determined by the use of St. Severin as an age monitor in this study), if Pu and U were not chemically fractionated in the Moon relative to St. Severin. Reasonable agreement is also obtained by comparison with the $^{136}Xe_{PF}/^{136}Xe_{UF}$ ratio of 0.6 determined for rock 14321 (Marti *et al.*, 1973a), for which Rb–Sr studies indicate an age near 4.00 b.y., although complete equilibration apparently did not occur during the final assembly of the breccia (Mark *et al.*, 1973). (Rock 14321 also has terrestrial-type trapped Xe.) Goswami and Hutcheon (1975) have identified $^{244}Pu$ fission tracks in a whitlockite crystal from rock 72255 in relative proportions of 0.5:1 with tracks from spontaneous fission of $^{238}U$. (A third source of fission tracks, cosmic-ray induced fission of Th and U, accounts for ~12% of the natural fission tracks implying that a somewhat smaller fraction (<5%) of the fissiogenic $^{136}Xe$ observed in Boulder 1 samples can be from this source, since Th/U ratios are much lower in whole-rock samples than in whitlockite.) While the fission track

ratio is a factor of two lower than the best estimate of $^{136}Xe_{PF}/^{136}Xe_{UF}$, this difference could be explained by partial annealing of fission tracks in the whitlockite during the early history of Boulder 1. Thus three independent estimates of the expected $^{136}Xe_{PF}/^{136}Xe_{UF}$ are in approximate agreement with the 1:1 proportions implied by our analysis of the data in Figure 8. Uncertainties in the allowable cosmogenic $^{129}Xe/^{130}Xe$ ratios and in the relative abundances of Xe and U lead us to accept a range of probable values given by $^{136}Xe_{PF}/^{136}Xe_{UF}=1.0\pm0.4$. This range includes the estimate from St.Severin on the high end and the 14321 value on the low end, and also overlaps with the uncertainties in the $^{244}Pu/^{238}U$ fission track ratio for the whitlockite from 72255. In Figure 9, we again plot $^{136}Xe$ against $^{129}Xe$, but renormalized to $^{126}Xe$. In this plot the 'fission-corrected' points were obtained by subtracting the contributions from $^{244}Pu$ and $^{238}U$ using $^{136}Xe_{PF}/^{136}Xe_{UF}=1.0\pm0.4$, with the result that all of the plotted 'fission-corrected' points (including the LFBx) agree well with a mixture of cosmogenic Xe ($^{129}Xe/^{126}Xe\simeq1.6$) and trapped Xe of terrestrial composition. We emphasize that a solar-type trapped component such as SUCOR (Podosek *et al.*, 1971) can now be ruled out for both high-temperature and low-temperature extractions. To our knowledge, these are the first Apollo 17 samples to be added to the

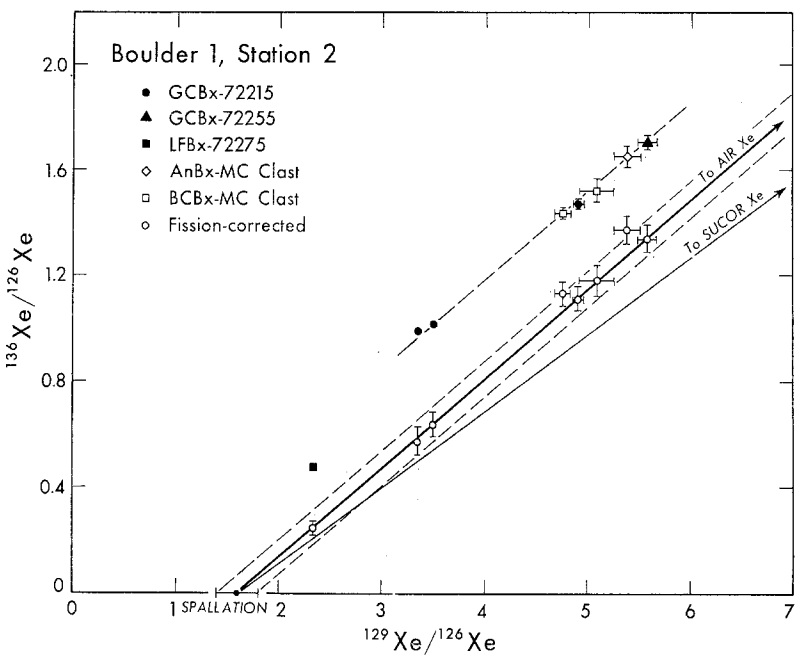


Fig. 9. Isotopic correlation of $^{136}Xe/^{126}Xe$ with $^{129}Xe/^{126}Xe$. Only total high-temperature data (1650 or 1100+1650°C) are shown. Open circles have been corrected for $^{136}Xe$ from spontaneous fission *in situ* of both $^{238}U$ and $^{244}Pu$ with $^{136}Xe_{PF}/^{136}Xe_{UF}\equiv1.0\pm0.4$. The dark solid line flanked by dashed lines represents a two-component mixture of AIR Xe and Xe from spallation with $^{136}Xe/^{126}Xe\equiv0.0032$ (R. C. Reedy, personal communication, 1975) and $^{129}Xe/^{126}Xe=1.6\pm0.2$. (The continuation of the upper dashed line is also constrained to pass through the AIR point.) The light solid line represents a similar mixture with SUCOR instead of AIR as the trapped component.

growing list of lunar rocks exhibiting high-temperature release of terrestrial-type Xe.

The trapped $^{84}Kr$ and $^{132}Xe$ abundances determined from the above analyses and plotted in Figure 6 correlate quite well, as $^{84}Kr/^{132}Xe$ ratios vary by only a factor of two. Using trapped $^{20}Ne$ as an indicator of solar-wind contamination, we can conclude that only a small to negligible fraction of the trapped Kr and Xe can be from this source. The relative elemental abundances of trapped $^{36}Ar$, Kr, and Xe are similar to values reported for rock 60015 (Leich and Niemeyer, 1975) except for some excesses of $^{36}Ar$ which can be attributed to solar-wind contamination. Lightner and Marti (1974) have suggested that a correlation of terrestrial-type trapped Xe abundances with other lunar volatiles would be a strong argument in favor of a lunar origin for the trapped Xe. Comparison with volatile element data from Morgan *et al.* (1976) shows that some correlations can be made, but that there are always a few samples which deviate from the general trend. For example, the BCBx samples from Marble Cake have the highest Br and trapped Xe abundances, the 72255 GCBx is intermediate, and most other samples have significantly lower Br and trapped Xe abundances. However, the CN samples from Civet Cat do not fit the correlation at all, with two other samples showing smaller, but still significant, deviations. In general, the volatile-element data do suggest the correlations which might indicate a lunar origin for the trapped Xe, but the correlations are not strong enough to form the basis for a convincing argument. Consequently, we offer no further speculations concerning the origin of the trapped component.

## 5. Cosmic Ray Exposure History

Estimates of cosmic-ray exposure age can be made from rare gas data by two fundamentally different methods. The first method is simply to divide the measured abundances of selected cosmogenic isotopes by the appropriate 'average' production rates. However, exposure ages derived in this way are subject to sizable uncertainties in the rare gas abundance measurements and even greater uncertainties due to variable production rates. The $^{81}Kr$–Kr method avoids both of these sources of error by allowing the calculation of an exposure age directly from the relative abundances of the cosmogenic Kr isotopes, including the radioactive ($\lambda_{81} = 3.3 \times 10^{-6}$ y$^{-1}$) isotope $^{81}Kr$ (Marti, 1967). Consequently $^{81}Kr$–Kr exposure ages are much more reliable for samples with a simple exposure history.

Cosmogenic Kr isotopic spectra (Table III) were calculated for each sample using the data from the 1650° (or 1100° + 1650° for 72275,57 and 72275,166) temperature step, according to the Kr decomposition procedures described in the preceding section. Uncertainties were compounded quadratically at each step of the calculation. In the absence of anomalies at $^{80,82}Kr$ (from neutron capture by Br), the relative production rates of $^{81}Kr$ and $^{83}Kr$ can be evaluated using the equation

$$\frac{P_{81}}{P_{83}} = \frac{0.95}{2}\left[\left(\frac{^{80}Kr}{^{83}Kr}\right)_c + \left(\frac{^{82}Kr}{^{83}Kr}\right)_c\right] \quad (1)$$

TABLE III

Cosmogenic krypton isotopic spectra[a] and relative production rates of $^{81}Kr$ and $^{83}Kr$

| Sample | $^{83}Kr$ ($\times 10^{-12}$ cm$^3$ STP g$^{-1}$) | $^{78}Kr$ | $^{80}Kr$ | $^{81}Kr$ | $^{82}Kr$ | $^{84}Kr$ | $P_{81}$ |
|---|---|---|---|---|---|---|---|
| | | $^{83}Kr \equiv 100$ | | | | | $P_{83}$ |
| 72215,60 | 73 | 19.07 | 51.1 | 0.431 | 76.6 | 39.4 | 0.607 |
| (GCBx) | ±7 | ±0.35 | ±0.6 | ±0.028 | ±0.8 | ±4.6 | |
| 72215,64 | 64 | 18.82 | 50.9 | 0.410 | 76.6 | 40.1 | 0.606 |
| (GCBx) | ±7 | ±0.41 | ±0.7 | ±0.031 | ±0.9 | ±4.7 | |
| 72215,92 | 75 | 19.45 | 50.6 | 0.457 | 76.2 | 37.5 | 0.602 |
| (GCBx) | ±8 | ±0.32 | ±0.7 | ±0.020 | ±1.2 | ±4.7 | |
| 72255,42 | 36 | 15.8 | 44.2 | 0.33 | 73 | 50 | 0.559 |
| (CN) | ±7 | ±2.3 | ±7.6 | ±0.19 | ±11 | ±11 | |
| 72255,52 | 66 | 19.45 | 51.4 | 0.417 | 76.2 | 38.6 | 0.606 |
| (GCBx) | ±10 | ±0.43 | ±1.1 | ±0.031 | ±1.6 | ±4.9 | |
| 72275,57 | 108 | 21.84 | 53.9 | 0.360 | 76.9 | 38.3 | 0.622 |
| (LFBx) | ±11 | ±0.32 | ±0.7 | ±0.013 | ±0.6 | ±5.3 | |
| 72275,76 | 124 | 18.94 | 52.6 | 0.349 | 77.9 | 35.9 | 0.620 |
| (AnBx) | ±14 | ±0.77 | ±1.8 | ±0.047 | ±2.8 | ±5.2 | |
| 72275,80 | 151 | 20.84 | 58.1 | 0.334 | 80.0 | 35.5 | 0.617 |
| (BCBx) | ±17 | ±1.18 | ±3.4 | ±0.055 | ±4.5 | ±5.5 | |
| 72275,91 | 83 | 15.2 | 51 | 0.24 | 78 | 32 | 0.613 |
| (PB) | ±33 | ±7.7 | ±27 | ±0.15 | ±39 | ±15 | |
| 72275,166 | 188 | 20.92 | 61.1 | 0.357 | 81.3 | 40.6 | 0.617 |
| (BCBx) | ±27 | ±0.40 | ±0.8 | ±0.016 | ±0.7 | ±7.2 | |

[a] Calculated assuming cosmogenic $^{86}Kr/^{83}Kr = 0.15 \pm 0.15$ and trapped Kr of BEOC 12 (Eberhardt *et al.*, 1972) composition.

(Marti *et al.*, 1970). The dashed line in Figure 10, determined by the data for the 72215 GCBx and 72275 LFBx samples, is similar to the expected correlation of purely spallogenic Kr resulting from variations in targer element chemistry ($Zr/Sr \sim 3$ for GCBx and $\sim 6$ for LFBx from Table II). The general agreement with this trend indicates that neutron capture effects are not important for most samples. Only the BCBx samples show a clear excess of $^{80}Kr$ in Figure 10. A similar analysis indicates corresponding excesses of $^{82}Kr$ in the BCBx samples, confirming the identification with production from Br by neutron capture. The BCBx samples are exceptional in this regard because Br is enriched in these samples by a factor of six relative to the LFBx and a factor of ten relative to the 72215 GCBx (Morgan *et al.*, 1975). However, lack of any indication of excess $^{80,82}Kr$ in the 72255 GCBx sample, with approximately one-third the Br content and one-half the spallogenic Kr abundance of the 72275 BCBx samples, suggests a lower lunar neutron fluence for rock 72255 than for rock 72275.

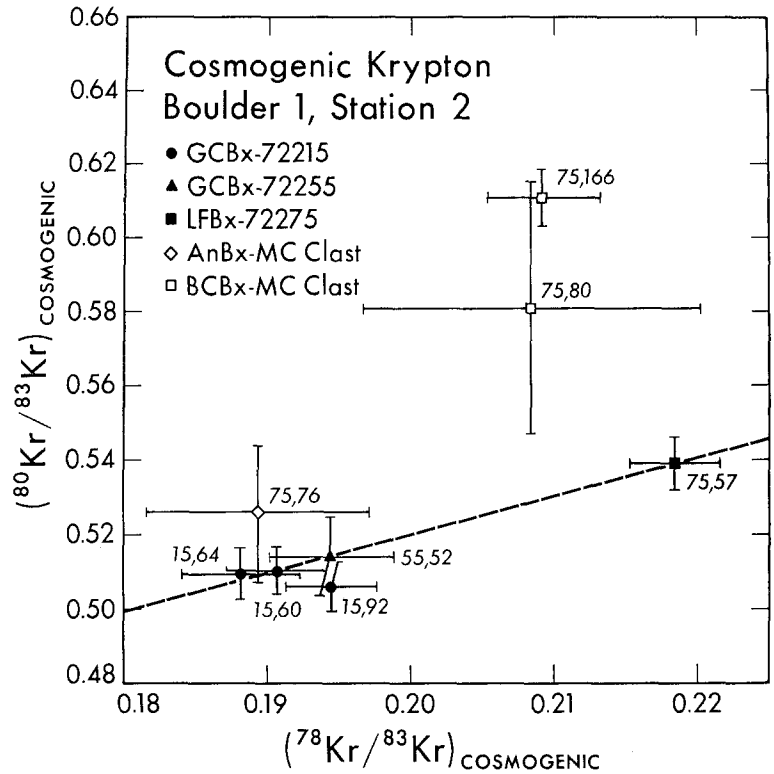


Fig. 10. Three-isotope plot of cosmogenic Kr. Compositional variations along the dashed line can be accounted for by variations in relative abundances of target elements (primarily Sr and Zr) for production of Kr from spallation. The vertical displacement of the two BCBx points indicates a contribution to $^{80}Kr$ from lunar neutron capture by $^{79}Br$.

The relative production rates of $^{81}Kr$ and $^{83}Kr$ ($P_{81}/P_{83}$) given in Table III were calculated from Equation (1), except for the BCBx samples, where cosmogenic $^{78}Kr/^{83}Kr$ ratios were used to interpolate between the production rates for the LFBx and GCBx samples. Exposure ages were then calculated from the equation

$$T \simeq \frac{1}{\lambda_{81}} \frac{P_{81}}{P_{83}} \left( \frac{^{83}Kr}{^{81}Kr} \right)_c , \tag{2}$$

which is valid for $T \gg 1/\lambda_{81}$ (Marti, 1967). The resulting $^{81}Kr$–Kr exposure ages are presented graphically in Figure 11. (Ages calculated for the PB and CN samples are unreliable due to large uncertainties in the cosmogenic $^{81}Kr/^{83}Kr$ ratios and have been omitted.) Good agreement is obtained for exposure ages calculated from samples of rocks 72215 and 72255, resulting in a weighted mean of 41.8 m.y. with a 1.3 m.y. standard deviation of the mean. However, a different $^{81}Kr$–Kr exposure age is clearly indicated for rock 72275, for which the weighted mean is 52.5 m.y. with a standard deviation of 1.4 m.y. Discordant exposure ages for samples from a single

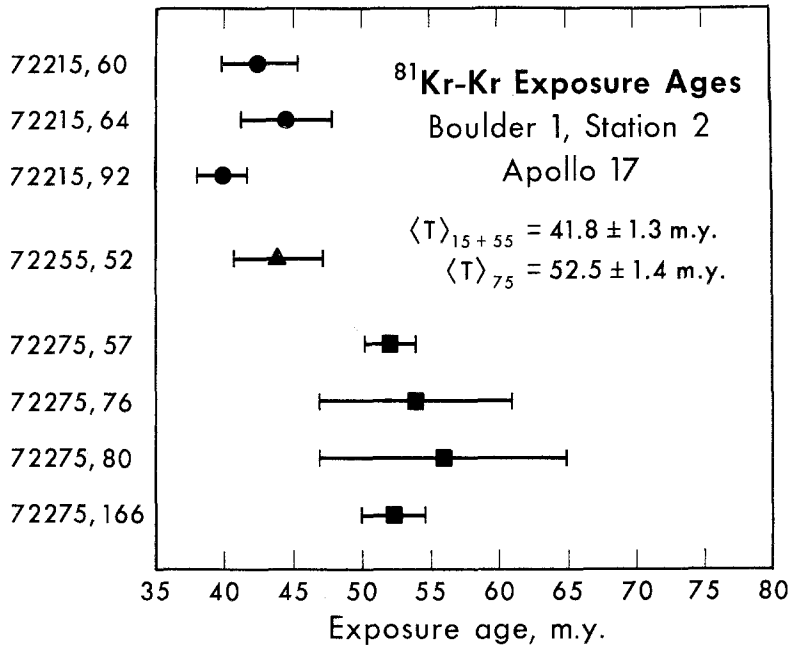


Fig. 11. $^{81}$Kr–Kr exposure ages. Mean exposure ages $\langle T \rangle$ for rocks 72215+72255 and for rock 72275 are 41.8±1.3 m.y. and 52.5±1.4 m.y., respectively. See text for discussion.

boulder must be explained by differences in shielding depth (past and present), since the various portions of the boulder certainly could not have been excavated from near the top of the South Massif at different times. In the discussion which follows we attempt to develop a self-consistent model of shielding history for these rocks using data for all cosmogenic gases, and to use this model to estimate the actual emplacement time for Boulder 1.

Estimating exposure ages from meteoritic production rates (corrected for $\sim 2\pi$ exposure geometry) for $^{38}$Ar, $^{83}$Kr, and $^{126}$Xe results in generally good agreement with the $^{81}$Kr–Kr exposure ages (Table IV). However, exposure ages derived from cosmogenic $^{3}$He and $^{21}$Ne are somewhat lower. Calculation of $^{38}$Ar–Ca exposure ages based on the correlated release of cosmogenic $^{38}$Ar and pile-produced $^{37}$Ar in the irradiated samples gives systematically higher results. This discrepancy can be traced to the BMS2 calibration problems discussed earlier, since the $^{38}$Ar–Ca exposure age calculation depends on this calibration through the $^{37}$Ar/Ca conversion ratio. Consequently, we regard the absolute exposure ages determined by the $^{38}$Ar–Ca technique to be unreliable; however, the exposure age ratio of 0.70±0.08 for rock 72255 relative to rock 72275 is a firm result, independent of the absolute calibration, and is in good agreement with the $^{81}$Kr–Kr exposure age ratio of 0.80±0.03 for rocks 72215 and 72255 relative to rock 72275.

The consistently lower cosmogenic abundance exposure ages for rocks 72215 and 72255 relative to rock 72275 imply average production rates for cosmogenic isotopes

~20% lower for rocks 72215 and 72255 than for rock 72275. However, the discordancy of the $^{81}$Kr–Kr ages by this same factor requires that recent production rates for $^{81}$Kr be the same for all three rocks, despite the apparently greater self-shielding of the samples from the side of the boulder (72215 and 72255) compared with the exposed location of rock 72275 at the top. Thus the lower average production rates for rocks 72215 and 72255 cannot be attributed to the effects of self-shielding by the boulder in its present orientation. We therefore conclude that a prior exposure

TABLE IV

Cosmic ray exposure ages (m.y.)

| Method | Rock Number | | |
|---|---|---|---|
| | 72215 | 72255 | 72275 |
| $^{81}$Kr–Kr | 41.4 | 44.1 | 52.5 |
| $^{38}$Ar–Ca | – | 52 | 74 |
| $^{3}$He | 16 | 26 | 38 |
| $^{21}$Ne | 26 | 27 | 33 |
| $^{38}$Ar | 41 | 41 | 50 |
| $^{83}$Kr | (36) | 34 | 44 |
| $^{126}$Xe | (49) | 52 | 64 |

For method of calculation of $^{81}$Kr–Kr exposure ages, see text. All other exposure ages calculated from meteoritic production rates (corrected for an assumed $2\pi$ exposure geometry) tabulated by Eberhardt *et al.* (1974). Ages in parentheses were calculated assuming the target element composition measured in GCBx sample 72255,52 (Table II).

under different shielding conditions, characterized by distinctly lower cosmogenic production rates for rocks 72215 and 72255, must account for a significant fraction of the observed cosmogenic abundances.

Perhaps the most sensitive rare gas indicator of shielding variations is the cosmogenic $^{131}$Xe/$^{126}$Xe ratio, because of the rather large resonance integral for neutron capture by $^{130}$Ba, with $^{131}$Xe as the stable product (Browne and Berman, 1972). We have calculated cosmogenic Xe spectra (Table V) from the isotopic data using the terrestrial atmospheric composition (Nier, 1950) for the trapped Xe, and a fissiogenic component from spontaneous fission *in situ* of $^{238}$U (Wetherill, 1953) and $^{244}$Pu (Alexander *et al.*, 1971), as justified in the previous section. We also assume a value of $0.0032 \pm 0.0016$ for the cosmogenic $^{136}$Xe/$^{126}$Xe ratio, based on calculations by R. C. Reedy (personal communication, 1975); however this assumption is not a critical one, as the calculated cosmogenic Xe ratios are essentially unchanged if the relative cosmogenic $^{136}$Xe yield is as much as five times the assumed value. Model-dependent effects on calculated cosmogenic yields are relatively small for $^{128,130,131}$Xe and virtually nonexistent for $^{124,126}$Xe, so ratios involving these isotopes are the most reliable. In general, calculated ratios are in good agreement with correlations based

TABLE V

Isotopic spectra of cosmogenic Xe [a]

| Sample | $^{126}$Xe ($\times 10^{-12}$ cm$^3$ STP g$^{-1}$) | $^{124}$Xe | $^{128}$Xe | $^{129}$Xe | $^{130}$Xe | $^{131}$Xe | $^{132}$Xe | $^{134}$Xe |
|---|---|---|---|---|---|---|---|---|
| | | $^{126}$Xe≡1 | | | | | | |
| 72215,60 (GCBx) | 14.6 ±1.5 | 0.560 ±0.008 | 1.519 ±0.025 | 1.64 ±0.29 | 1.028 ±0.046 | 4.44 ±0.21 | 0.82 ±0.22 | 0.041 ±0.029 |
| 72215,64 (GCBx) | 14.4 ±1.6 | 0.568 ±0.008 | 1.542 ±0.024 | 1.61 ±0.25 | 1.048 ±0.041 | 4.51 ±0.19 | 0.81 ±0.19 | 0.045 ±0.028 |
| 72215,92 (GCBx) | 15.5 ±1.6 | 0.563 ±0.005 | 1.511 ±0.022 | 1.62 ±0.27 | 1.027 ±0.042 | 4.44 ±0.19 | 0.80 ±0.20 | 0.046 ±0.027 |
| 72255,42 (CN) | 6.3 ±0.8 | 0.583 ±0.043 (0.584) | 1.56 ±0.11 (1.59) | 1.11 ±0.27 (1.56) | 1.032 ±0.085 (1.100) | 4.07 ±0.33 (4.39) | 0.65 ±0.20 (0.97) | 0.040 ±0.120 (0.079) |
| 72255,52 (GCBx) | 16.5 ±1.7 | 0.554 ±0.016 | 1.484 ±0.035 | 1.62 ±0.26 | 0.977 ±0.043 | 3.97 ±0.20 | 0.78 ±0.19 | 0.050 ±0.030 |
| 72275,57 (LFBx) | 28.1 ±2.9 | 0.580 ±0.009 | 1.483 ±0.023 | 1.61 ±0.16 | 0.943 ±0.027 | 4.51 ±0.13 | 0.78 ±0.12 | 0.049 ±0.015 |
| 72275,76 (AnBx) | 24.2 ±2.6 | 0.562 ±0.016 | 1.519 ±0.044 | 1.33 ±0.20 | 0.930 ±0.039 | 4.44 ±0.18 | 0.55 ±0.15 | 0.025 ±0.027 |
| 72275,80 (BCBx) | 39.7 ±4.4 | 0.582 ±0.020 | 1.553 ±0.062 | 1.60 ±0.26 | 1.011 ±0.051 | 4.64 ±0.27 | 0.81 ±0.18 | −0.011 ±0.048 |
| 72275,91 (PB) | 22.5 ±4.8 | 0.61 ±0.11 | 1.58 ±0.29 | 1.82 ±0.35 | 1.00 ±0.17 | 4.97 ±0.86 | 0.90 ±0.21 | 0.063 ±0.041 |
| 72275,166 (BCBx) | 47.2 ±4.9 | 0.578 ±0.012 | 1.484 ±0.033 | 1.41 ±0.21 | 0.961 ±0.037 | 4.53 ±0.17 | 0.69 ±0.16 | 0.035 ±0.022 |

[a] Calculated assuming cosmogenic $^{136}Xe/^{126}Xe = 0.0032 \pm 0.0016$ (R. C. Reedy, personal communication, 1975), a terrestrial atmospheric composition for the trapped Xe, and fissiogenic Xe from *in situ* spontaneous fission of $^{244}$Pu and $^{238}$U, with $^{136}Xe_{PF}/^{136}Xe_{UF} = 1.0 \pm 0.4$. Numbers in parentheses were calculated for $^{136}Xe_{PF}/^{136}Xe_{UF} \equiv 2.0$.

on much wider variations in lunar cosmogenic Xe compositions (Podosek and Huneke, 1971). The slight systematic differences between the LFBx and BCBx from rock 72275 on the one hand and the 72215 GCBx on the other (i.e. higher $^{124}Xe/^{126}Xe$ and lower $^{128,130}Xe/^{126}Xe$ for rock 72275) indicate either greater average shielding conditions or higher Ba/REE ratios for rock 72215 than for rock 72275. As of this writing we can only estimate Ba/REE ratios using Ba abundances from Table II and REE abundances from Blanchard *et al.* (1974). Although the resulting Ba/REE may well be unreliable due to sample inhomogeneities, we do indeed find a slightly higher Ba/REE ratio for the GCBx from rock 72255 (which is very similar to the 72215 GCBx) than for any of the 72275 samples. Thus we conclude that small variations in target-element chemistry may account for the slight systematic differences in the purely spallogenic Xe yields. At least some of the scatter, especially for $^{129}$Xe, can be

attributed to a necessarily oversimplified Xe decomposition model. A case in point is the low $^{129}Xe$ yield indicated for the Civet Cat (CN) sample. A cosmogenic Xe composition more consistent with the majority of other samples can be obtained by assuming a higher $^{136}Xe_{PF}/^{136}Xe_{UF}$ ratio ($\sim 2$) for the Civet Cat, as a relic of an igneous age somewhat greater than 4.0 b.y. (Compston *et al.*, 1975). However a 50% higher U content for this sample than for the small aliquot used for the U measurement cannot be entirely ruled out, and would have essentially the same effect on the Xe decomposition.

The general agreement of cosmogenic $^{131}Xe/^{126}Xe$ ratios appears to rule out the possibility of resolving shielding differences from this indicator. The lack of a correlation between cosmogenic $^{78}Kr/^{83}Kr$ and $^{131}Xe/^{126}Xe$ ratios in Figure 12 is the result of variations in target element chemistry (mainly the Zr/Sr ratio) with only the low $^{131}Xe/^{126}Xe$ ratio for the 72255 GCBx sample suggesting a more shielded location for rock 72255 than for rocks 72215 and 72275. However, a closer scrutiny does imply distinct differences in the lunar neutron fluences for all three rocks. We first note that variations in purely spallogenic $^{131}Xe/^{126}Xe$ ratios (with typical values close to 3.0) are predictable from correlations with other spallogenic Xe ratios (Marti *et al.*, 1973b), implying somewhat smaller spallogenic $^{131}Xe/^{126}Xe$ values in the 72275 samples than in the samples from rocks 72215 and 72255. A more tangible factor is the $\sim 20\%$ lower specific concentration of spallation products for rocks 72215 and 72255 compared to rock 72275. Both of the above factors contribute to the conclusion

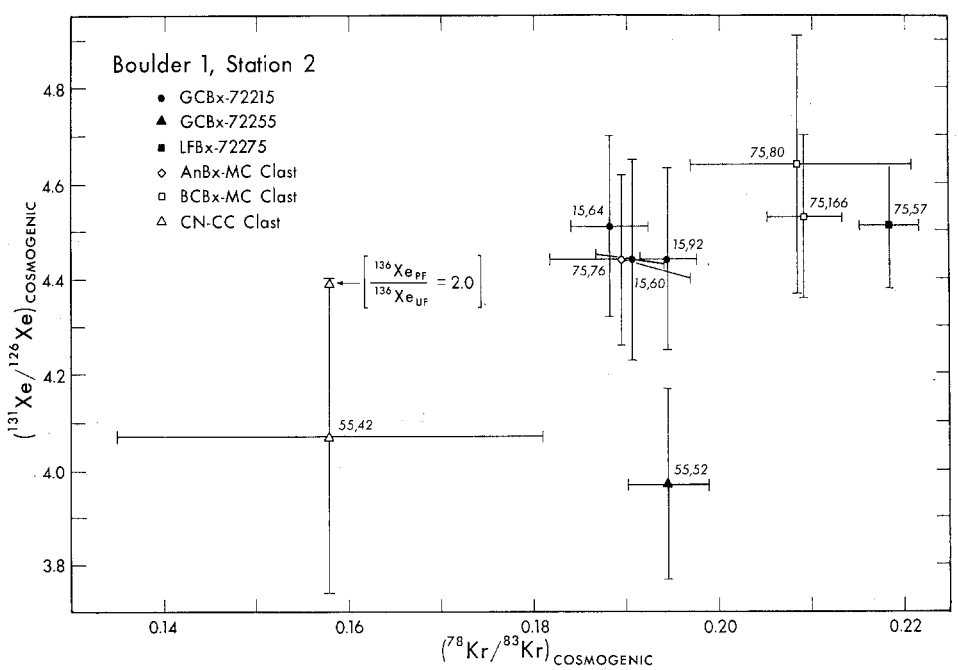


Fig. 12. Cosmogenic $^{131}Xe/^{126}Xe$ vs $^{78}Kr/^{83}Kr$. Calculations assuming $^{136}Xe_{PF}/^{136}Xe_{UF} \equiv 1.0 \pm 0.4$ (Table V) were used in all cases; however, the position of the point for CN sample 72255,42, assuming $^{136}Xe_{PF}/^{136}Xe_{UF} = 2.0$, is also shown. Error bars include the uncertainty assigned to this parameter.

that, in spite of the nearly identical cosmogenic $^{131}Xe/^{126}Xe$ ratios for rocks 72215 and 72275, the specific concentration of neutron-produced $^{131}Xe$ relative to Ba is distinctly lower, thereby implying a lower neutron fluence, for 72215 than for 72275. An even lower fluence for rock 72255 is required by the low cosmogenic $^{131}Xe/^{126}Xe$ for GCBx sample 72255,52. The lower neutron fluence postulated for rock 72255 relative to rock 72275 on the basis of neutron capture effects at $^{80,82}Kr$ is consistent with this conclusion.

Based on the evidence outlined above, we estimate a lunar neutron fluence for rock 72255 of roughly one-half the fluence for rock 72275, with an intermediate value implied for rock 72215. These conditions can be met by a two-state exposure model in which the bulk of the neutron exposure is accumulated in the first stage. A shielding depth placing rock 72275 near or below the lunar neutron flux maximum at $\sim 150$ g cm$^{-1}$ (Lingenfelter *et al.*, 1972; Woolum and Burnett, 1974), with successively greater shielding depths for rocks 72215 and 72255, appears to satisfy this requirement.

An independent test of such a model is made possible by the depth-dependent production rates for cosmogenic $^{3}He$, $^{21}Ne$ and $^{38}Ar$ derived from the Apollo 15 deep core by Pepin *et al.* (1974). Using these production rates, apparently discordant exposure ages based on 'average' production rates for these isotopes (Table IV) can be brought into reasonable agreement by a suitable model of shielding conditions. The $^{3}He$ abundances for rock 72215 are too low to fit any such model, but if these data are rejected the remaining cosmogenic abundances are in good agreement with a model which also fits the constraints implied by neutron capture effects discussed above. According to this model, which is not necessarily unique, the first stage of irradiation, lasting for $\sim 20$ m.y., was characterized by shielding depths of $\sim 100$ g cm$^{-2}$ for rock 72275 and $\sim 300$ g cm$^{-2}$ for rocks 72215 and 72255. The shielding conditions for the second and final stage are determined by the individual sampling depths ($\lesssim 15$ g cm$^{-1}$), with allowances for slow continual erosion. The duration of the final stage implied by this model is $\sim 35$ m.y., in reasonable agreement with the cosmic-ray track exposure age determined by Goswami and Hutcheon (1975) for rock 72255.

While the above model is quite adequate to explain the rare gas record of cosmic-ray interactions in Boulder 1, it may be possible to fit the data equally well with a longer first-stage exposure at correspondingly deeper burial depths. Work is continuing on refining exposure models of this type with the object of establishing additional chronological constraints. At present we can only conclude that the cosmic-ray exposure of the boulder began at a time $\gtrsim 55$ m.y. ago, and that a discrete change in shielding conditions occurred about 35 m.y. ago.

Since Boulder 1 rests on the light mantle adjacent to the South Massif, time constraints can be established for the emplacement of this feature as well as for the boulder itself. Photogeologic analyses summarized by Wolfe (1975) have associated the emplacement of the light mantle with the Tycho cratering-event, either as an avalanche initiated by Tycho ejecta or as the ejecta blanket from a cluster of Tycho secondary craters on the South Massif. Wolfe (1975) also argues that the boulder is not a part of the light mantle deposit and must therefore postdate the light mantle.

Thus a roughly defined lower limit of 35 m.y. can be placed on the time of emplacement of the light mantle. However, it seems quite probable that the event responsible for initiating the cosmic-ray exposure of Boulder 1 $\gtrsim$55 m.y. ago was the downward displacement of material initially covering the blocky area identified as the boulder source-crop to form the light mantle. Thus a somewhat more speculative lower limit of 55 m.y. can be placed on the age of Tycho and the emplacement of the light mantle. Following the excavation of the boulder source-crop, Boulder 1 probably remained in place until dislodged by a local impact 35 m.y. ago. It then rolled down the hill, shedding material on the way, and eventually came to rest in its present position. We favor this interpretation over an alternative one in which the excavation and emplacement of the boulder occurred in a single event ($\sim$55 m.y. ago) with a minor spalling event responsible for the later shielding change. The latter interpretation seems unlikely for two reasons. First, the amount of spalled material would have to be quite substantial ($\sim$1 m thickness), approaching the size of the boulder itself. Second, the geological model of the Boulder 1 site would then require three major events instead of just two: (1) emplacement of the light mantle, (2) excavation and emplacement of the boulder, and (3) fragmentation of the boulder *in situ*.

Without choosing a specific interpretation for the history of Boulder 1, we are still able to make two relatively firm conclusions. The first conclusion is that prior to $\sim$55 m.y. ago Boulder 1 still lay buried in the South Massif where it had been deposited by the Serenitatis impact. The second is that Boulder 1 has remained in its present configuration for the last $\sim$35 m.y.

## Acknowledgements

We would like to thank Prof. J. H. Reynolds for his guidance and criticism of this work and Prof. E. C. Alexander, Jr. for planning and executing the irradiation. Our thanks also go to the operational staff of the U.S. Geological Survey reactor facility and to H. Michel of the Lawrence Berkeley Laboratory for their assistance with various aspects of the irradiation. We are indebted to N. J. Hubbard, M. Bansal, and H. Weismann for performing the chemical analyses and supplying us with their first results. We have benefited greatly from discussions with the members of Consortium Indomitabile. Finally, we thank G. McCrory for his invaluable technical support, R. Moniot for his assistance with the data analysis, and E. Keyser for her skill and patience in the preparation of this manuscript.

## Data Appendix

TABLE A.1

Argon abundances* and isotopic ratios in pile-irradiated samples from Boulder 1, Station 2

| 72255,42† | | 0.1277 g | | | |
|---|---|---|---|---|---|
| Temperature | $^{40}Ar$ | $^{36}Ar/^{40}Ar$ | $^{37}Ar/^{40}Ar$ | $^{38}Ar/^{40}Ar$ | $^{39}Ar/^{40}Ar$ |
| (°C) | ($\times 10^{-8}$ cm$^3$ STP g$^{-1}$) | ($\times 10^{-5}$) | | | |
| 400 | 4.0±5.0 | 0.0±1000.0 | 4700.0±6200.0 | 270.0±280.0 | 210.0±300.0 |
| 500 | 117.0±5.0 | 106.0±17.0 | 1696.0±87.0 | 46.8±2.8 | 213.0±10.0 |
| 600 | 677.0±6.0 | 48.2±2.9 | 3969.0±40.0 | 36.9±4.1 | 240.1±2.1 |
| 700 | 1038.0±7.0 | 59.2±2.2 | 4203.0±35.0 | 37.0±1.0 | 197.0±1.1 |
| 800 | 1117.0±7.0 | 78.2±3.4 | 6186.0±50.0 | 53.9±0.9 | 183.9±1.1 |
| 900 | 1115.0±7.0 | 49.7±1.8 | 6986.0±56.0 | 58.8±0.4 | 184.8±1.0 |
| 1000 | 1305.0±7.0 | 52.8±1.5 | 7806.0±60.0 | 62.6±0.6 | 185.4±0.9 |
| 1100 | 895.0±6.0 | 59.9±2.3 | 7522.0±87.0 | 63.3±0.7 | 189.3±1.5 |
| 1200 | 2492.0±12.0 | 61.1±1.0 | 8517.0±61.0 | 68.9±0.8 | 184.2±0.6 |
| 1400 | 3148.0±14.0 | 53.4±1.2 | 8770.0±66.0 | 68.7±0.5 | 179.9±0.7 |
| 1600 | 27.0±5.0 | 134.0±58.0 | 6900.0±1400.0 | 144.0±28.0 | 181.0±47.0 |
| Total | 11935.0±26.0 | 58.3±0.7 | 7365.0±25.0 | 60.8±0.4 | 188.2±0.4 |

† Fluence relative to age monitor = 0.994±0.006.

* An additional uncertainty of ±10% in the absolute calibrations should be applied to the abundance data.

| 72255,52† | | 0.1399 g | | | |
|---|---|---|---|---|---|
| Temperature | $^{40}Ar$ | $^{36}Ar/^{40}Ar$ | $^{37}Ar/^{40}Ar$ | $^{38}Ar/^{40}Ar$ | $^{39}Ar/^{40}Ar$ |
| (°C) | ($\times 10^{-8}$ cm$^3$ STP g$^{-1}$) | ($\times 10^{-5}$) | | | |
| 400 | 17.0±5.0 | 50.0±140.0 | 2260.0±860.0 | 50.0±140.0 | 300.0±140.0 |
| 500 | 302.0±5.0 | 76.3±6.8 | 1425.0±30.0 | 26.9±2.1 | 356.0±17.0 |
| 600 | 1430.0±8.0 | 87.9±1.2 | 2372.0±16.0 | 34.1±0.7 | 265.0±1.3 |
| 700 | 3301.0±12.0 | 170.2±0.9 | 2628.0±19.0 | 49.8±0.2 | 197.5±0.4 |
| 800 | 2078.0±9.0 | 163.1±1.2 | 2950.0±18.0 | 51.2±0.3 | 184.9±0.8 |
| 900 | 2463.0±14.0 | 52.3±1.0 | 3442.0±21.0 | 33.0±0.7 | 185.5±1.1 |
| 1000 | 2132.0±14.0 | 51.4±1.0 | 3715.0±26.0 | 38.6±0.5 | 186.7±1.0 |
| 1100 | 2058.0±10.0 | 87.6±0.9 | 5312.0±32.0 | 58.8±0.3 | 200.1±0.6 |
| 1200 | 1849.0±9.0 | 64.9±1.2 | 7135.0±50.0 | 67.2±0.4 | 198.7±1.0 |
| 1400 | 3313.0±12.0 | 53.1±1.0 | 7074.0±40.0 | 62.5±0.7 | 187.7±0.7 |
| 1600 | 23.0±5.0 | 235.0±38.0 | 3680.0±760.0 | 29.7±7.0 | 149.0±31.0 |
| Total | 18966.0±33.0 | 93.3±0.4 | 4361.0±11.0 | 49.8±0.2 | 199.7±0.4 |

† Fluence relative to age monitor = 1.004±0.006.

*Table A.1 (Continued)*

| 72275,57† | | 0.0874 g | | | |
|---|---|---|---|---|---|
| Temperature | $^{40}Ar$ | $^{36}Ar/^{40}Ar$ | $^{37}Ar/^{40}Ar$ | $^{38}Ar/^{40}Ar$ | $^{39}Ar/^{40}Ar$ |
| (°C) | ($\times 10^{-8}$ cm$^3$ STP g$^{-1}$) | ($\times 10^{-5}$) | | | |
| 400 | 13.0±8.0 | 270.0±150.0 | 5600.0±3400.0 | 160.0±80.0 | 890.0±550.0 |
| 500 | 230.0±8.0 | 60.0±13.0 | 3110.0±110.0 | 48.1±2.2 | 789.0±29.0 |
| 600 | 2659.0±14.0 | 29.8±1.3 | 2890.0±18.0 | 33.3±0.3 | 290.9±1.3 |
| 700 | 3593.0±18.0 | 20.9±1.2 | 2528.0±14.0 | 28.8±0.3 | 202.4±0.9 |
| 800 | 3085.0±16.0 | 24.5±1.2 | 2691.0±15.0 | 31.0±0.4 | 188.0±0.8 |
| 900 | 1867.0±11.0 | 28.1±1.7 | 2901.0±20.0 | 41.3±0.5 | 192.3±1.0 |
| 1000 | 1510.0±10.0 | 60.0±2.0 | 4020.0±30.0 | 93.8±0.7 | 223.4±1.3 |
| 1100 | 2466.0±13.0 | 74.4±1.1 | 7238.0±46.0 | 106.0±0.5 | 234.6±1.0 |
| 1200 | 1303.0±9.0 | 74.8±2.3 | 8154.0±68.0 | 98.6±0.6 | 197.3±1.3 |
| 1400 | 1457.0±10.0 | 79.0±2.4 | 8784.0±67.0 | 104.6±1.0 | 193.4±1.5 |
| 1600 | 151.0±8.0 | 75.0±20.0 | 8200.0±430.0 | 98.9±3.0 | 188.0±11.0 |
| Total | 18334.0±39.0 | 43.5±0.6 | 4356.0±13.0 | 58.7±0.2 | 224.5±0.8 |

† Fluence relative to age monitor = 1.008±0.006.

| 72275,76† | | 0.0781 g | | | |
|---|---|---|---|---|---|
| Temperature | $^{40}Ar$ | $^{36}Ar/^{40}Ar$ | $^{37}Ar/^{40}Ar$ | $^{38}Ar/^{40}Ar$ | $^{39}Ar/^{40}Ar$ |
| (°C) | ($\times 10^{-8}$ cm$^3$ STP g$^{-1}$) | ($\times 10^{-5}$) | | | |
| 400 | 17.0±9.0 | 55.0±190.0 | 6030.0±3160 | 46.0±22.0 | 760.0±420.0 |
| 500 | 283.0±9.0 | 63.0±17.0 | 4800.0±150.0 | 54.0±5.0 | 820.0±28.0 |
| 600 | 2478.0±13.0 | 55.7±1.4 | 6058.0±37.0 | 62.9±0.7 | 330.4±2.3 |
| 700 | 4309.0±19.0 | 43.9±0.8 | 4125.0±25.0 | 47.2±0.5 | 199.5±0.6 |
| 800 | 4446.0±22.0 | 39.1±1.2 | 3087.0±20.0 | 36.0±0.2 | 190.6±0.5 |
| 900 | 3529.0±17.0 | 22.6±1.0 | 1972.0±11.0 | 27.0±0.6 | 189.0±0.6 |
| 1000 | 2245.0±66.0 | 28.0±5.2 | 2170.0±64.0 | 33.8±1.2 | 240.4±7.1 |
| 1100 | 3806.0±19.0 | 47.8±0.9 | 4109.0±23.0 | 58.2±0.2 | 212.3±1.1 |
| 1200 | 1433.0±11.0 | 59.5±3.0 | 4576.0±40.0 | 61.3±1.0 | 189.4±1.3 |
| 1400 | 2254.0±13.0 | 72.6±1.4 | 8067.0±54.0 | 92.4±0.5 | 185.2±0.9 |
| 1600 | 43.0±9.0 | 0.0±315.0 | 4300.0±890.0 | 82.0±14.0 | 137.0±51.0 |
| Total | 24843.0±81.0 | 44.0±0.9 | 4040.0±13.0 | 49.4±0.2 | 220.6±0.9 |

† Fluence relative to age monitor = 1.004±0.006.

*Table A.1 (Continued)*

| 72275,80 † | | 0.1199 g | | | |
|---|---|---|---|---|---|
| Temperature | $^{40}Ar$ | $^{36}Ar/^{40}Ar$ | $^{37}Ar/^{40}Ar$ | $^{38}Ar/^{40}Ar$ | $^{39}Ar/^{40}Ar$ |
| (°C) | ($\times 10^{-8}$ cm$^3$ STP g$^{-1}$) | ($\times 10^{-5}$) | | | |
| 400 | 13.0±5.0 | 248.0±74.0 | 0.0±50.0 | 0.0±50.0 | 150.0±100.0 |
| 500 | 176.0±5.0 | 45.0±13.0 | 0.0±10.0 | 6.0±6.0 | 173.0±11.0 |
| 600 | 1036.0±7.0 | 39.2±2.0 | 925.0±74.0 | 16.3±1.2 | 226.4±3.4 |
| 700 | 3745.0±19.0 | 67.1±1.8 | 1207.0±29.0 | 25.0±0.5 | 201.6±3.2 |
| 800 | 4976.0±70.0 | 135.2±2.2 | 1152.0±27.0 | 36.9±0.7 | 188.8±2.7 |
| 900 | 4794.0±24.0 | 147.3±2.5 | 1365.0±34.0 | 41.2±1.6 | 186.7±2.8 |
| 1000 | 3584.0±24.0 | 41.9±1.1 | 1623.0±35.0 | 27.9±0.7 | 186.0±2.7 |
| 1100 | 2753.0±15.0 | 40.5±1.0 | 2096.0±52.0 | 36.0±1.1 | 204.2±3.0 |
| 1200 | 3810.0±22.0 | 71.0±1.2 | 4314.0±93.0 | 61.7±0.9 | 224.1±3.3 |
| 1400 | 2764.0±14.0 | 54.4±1.4 | 4608.0±96.0 | 60.2±1.2 | 198.1±2.9 |
| 1600 | 46.0±5.0 | 103.0±36.0 | 0.0±20.0 | 101.0±13.0 | 224.0±34.0 |
| Total | 27697.0±86.0 | 85.5±0.7 | 2113.0±20.0 | 39.6±0.4 | 198.5±1.1 |

† Fluence relative to age monitor = 1.004±0.006.

| 72275,83 † | | 0.1211 g | | | |
|---|---|---|---|---|---|
| Temperature | $^{40}Ar$ | $^{36}Ar/^{40}Ar$ | $^{37}Ar/^{40}Ar$ | $^{38}Ar/^{40}Ar$ | $^{39}Ar/^{40}Ar$ |
| (°C) | ($\times 10^{-8}$ cm$^3$ STP g$^{-1}$) | ($\times 10^{-5}$) | | | |
| 400 | 53.0±6.0 | 102.0±36.0 | 1230.0±140.0 | 0.0±7.0 | 153.0±19.0 |
| 500 | 413.0±6.0 | 60.1±5.0 | 878.0±32.0 | 27.3±1.5 | 171.0±2.5 |
| 600 | 1877.0±8.0 | 30.0±1.2 | 2208.0±16.0 | 28.0±0.4 | 197.7±0.7 |
| 700 | 2941.0±11.0 | 29.1±0.8 | 2613.0±16.0 | 30.7±0.3 | 184.7±0.5 |
| 800 | 2510.0±11.0 | 28.6±1.1 | 2881.0±18.0 | 34.0±0.3 | 181.9±0.6 |
| 900 | 2025.0±13.0 | 32.0±1.3 | 3132.0±21.0 | 40.5±0.8 | 180.0±1.1 |
| 1000 | 1837.0±9.0 | 38.2±1.2 | 3809.0±38.0 | 50.1±1.2 | 191.7±1.2 |
| 1100 | 3187.0±12.0 | 54.8±0.9 | 5311.0±34.0 | 68.4±0.8 | 203.5±0.4 |
| 1200 | 1990.0±9.0 | 70.3±1.5 | 6350.0±50.0 | 80.8±0.8 | 196.4±0.9 |
| 1400 | 2729.0±10.0 | 70.3±0.8 | 7100.0±44.0 | 87.1±0.3 | 187.3±0.5 |
| 1600 | 36.0±6.0 | 149.0±54.0 | 5710.0±910 | 125.0±20.0 | 184.0±29.0 |
| Total | 19598.0±31.0 | 45.4±0.4 | 4183.0±12.0 | 52.8±0.2 | 190.0±0.3 |

† Fluence relative to age monitor = 1.004±0.006.

*Table A.1 (Continued)*

| 72275,91 † | | 0.1018 g | | | |
|---|---|---|---|---|---|
| Temperature | $^{40}Ar$ | $^{36}Ar/^{40}Ar$ | $^{37}Ar/^{40}Ar$ | $^{38}Ar/^{40}Ar$ | $^{39}Ar/^{40}Ar$ |
| (°C) | ($\times 10^{-8}$ cm$^3$ STP g$^{-1}$) | ($\times 10^{-5}$) | | | |
| 400 | 28.0±7.0 | 190.0±60.0 | 2600.0±600.0 | 26.0±36.0 | 470.0±110.0 |
| 500 | 178.0±7.0 | 69.0±13.0 | 2710.0±100.0 | 38.5±5.4 | 780.0±29.0 |
| 600 | 2788.0±11.0 | 30.9±1.1 | 3212.0±23.0 | 36.8±0.4 | 320.6±1.3 |
| 700 | 3910.0±14.0 | 28.1±0.9 | 2551.0±18.0 | 29.8±0.6 | 201.1±1.0 |
| 800 | 3278.0±13.0 | 27.3±1.3 | 2689.0±20.0 | 31.9±0.6 | 192.1±1.1 |
| 900 | 1637.0±8.0 | 33.8±2.6 | 3046.0±25.0 | 54.1±0.4 | 194.4±1.4 |
| 1000 | 1151.0±8.0 | 72.7±2.1 | 4247.0±38.0 | 117.1±0.7 | 225.9±1.6 |
| 1100 | 1740.0±8.0 | 101.4±1.4 | 10573.0±82.0 | 154.7±0.6 | 254.4±1.3 |
| 1200 | 796.0±7.0 | 101.9±2.9 | 14130.0±160.0 | 160.0±1.2 | 209.1±2.1 |
| 1400 | 848.0±7.0 | 101.7±2.9 | 12460.0±140.0 | 144.3±1.2 | 197.1±1.8 |
| 1600 | 85.0±7.0 | 150.0±25.0 | 10500.0±800.0 | 127.0±10.0 | 170.0±16.0 |
| Total | 16439.0±30.0 | 48.6±0.6 | 4822.0±18.0 | 66.0±0.3 | 233.0±0.7 |

† Fluence relative to age monitor = 1.003±0.006.

TABLE A.2

Abundances and isotopic ratios of light rare gases in samples from Boulder 1, Station 2

| Sample | Wt (g) | $^3He$ ($\times 10^{-8}$) | $^4He$ ($\times 10^{-4}$) | $^{22}Ne$ ($\times 10^{-8}$) | $^{20}Ne/^{22}Ne$ | $^{21}Ne/^{22}Ne$ | $^{36}Ar$ ($\times 10^{-8}$) | $^{38}Ar/^{36}Ar$ | $^{40}Ar/^{36}Ar$ |
|---|---|---|---|---|---|---|---|---|---|
| 72215,60 | 0.2673 | 16.5 | 9.7 | 4.28 | 0.996 | 0.829 | 4.30 | 1.252 | 2770 |
| (GCBx) | | ±1.2 | ±0.9 | ±0.21 | ±0.014 | ±0.004 | ±0.36 | ±0.011 | ±140 |
| 72215,64 | 0.2472 | 15.8 | 9.0 | 4.37 | 0.961 | 0.821 | 4.23 | 1.235 | 3155 |
| (GCBx) | | ±1.1 | ±0.9 | ±0.21 | ±0.010 | ±0.004 | ±0.36 | ±0.004 | ±163 |
| 72215,92 | 0.3132 | 16.0 | 9.8 | 4.16 | 0.799 | 0.836 | 4.17 | 1.296 | 2817 |
| (GCBx) | | ±1.1 | ±0.9 | ±0.20 | ±0.009 | ±0.004 | ±0.37 | ±0.004 | ±149 |
| 72255,42 | 0.0710 | 24.4 | 4.4 | 3.95 | 0.988 | 0.861 | 3.95 | 1.262 | 1703 |
| (CN) | | ±1.7 | ±0.8 | ±0.09 | ±0.068 | ±0.007 | ±0.20 | ±0.024 | ±86 |
| 72255,52 | 0.2312 | 27.3 | 12.0 | 6.45 | 2.844 | 0.699 | 7.59 | 0.737 | 1787 |
| (GCBx) | | ±2.1 | ±1.1 | ±0.33 | ±0.056 | ±0.004 | ±0.38 | ±0.011 | ±113 |
| 72275,57 | 0.4072 | 43.6 | 15.7 | 4.99 | 0.831 | 0.874 | 4.36 | 1.333 | 2488 |
| (LFBx) | | ±3.1 | ±1.2 | ±0.08 | ±0.061 | ±0.003 | ±0.22 | ±0.012 | ±155 |
| 72275,76 | 0.1425 | 26.1 | 13.2 | 4.09 | 1.48 | 0.774 | 6.63 | 1.114 | 2690 |
| (AnBx) | | ±1.8 | ±1.2 | ±0.08 | ±0.19 | ±0.006 | ±0.33 | ±0.014 | ±170 |
| 72275,80 | 0.0606 | 36.5 | 23.4 | 10.01 | 6.49 | 0.425 | 22.1 | 0.434 | 1288 |
| (BCBx) | | ±2.9 | ±2.4 | ±0.27 | ±0.16 | ±0.009 | ±1.1 | ±0.008 | ±81 |
| 72275,91 | 0.0339 | 50.1 | 11.6 | 5.07 | 1.080 | 0.879 | 5.24 | 1.230 | 2117 |
| (PB) | | ±5.1 | ±1.6 | ±0.18 | ±0.070 | ±0.009 | ±0.29 | ±0.035 | ±115 |
| 72275,166 | 0.1923 | 33.6 | 27.0 | 5.63 | 0.848 | 0.847 | 5.94 | 1.136 | 4434 |
| (BCBx) | | ±2.6 | ±2.3 | ±0.25 | ±0.086 | ±0.003 | ±0.29 | ±0.008 | ±263 |

Abundances are given in units of cm$^3$ STP g$^{-1}$. Errors include uncertainties in mass discrimination and blank corrections at the 1$\sigma$ level. An additional uncertainty of ±10% in the absolute calibrations should be applied to the abundance data.

TABLE A.3

Abundances and isotopic ratios of krypton in samples from Boulder 1, Station 2

| Sample | Temp. (°C) | $^{84}Kr$ ($10^{-12}$ cm$^3$ STP g$^{-1}$) | $^{78}Kr$ | $^{80}Kr$ | $^{81}Kr$ | $^{82}Kr$ | $^{83}Kr$ | $^{84}Kr$ | $^{86}Kr$ |
|---|---|---|---|---|---|---|---|---|---|
| 72215,60 | 700 | 52.7 | 1.17 | 5.84 | 0.021 | 22.55 | 23.80 | ≡100 | 30.28 |
| (GCBx) | | ±1.2 | ±0.02 | ±0.05 | ±0.019 | ±0.19 | ±0.14 | | ±0.23 |
| | 1650 | 116.5 | 12.06 | 34.02 | 0.262 | 61.88 | 76.12 | ≡100 | 24.42 |
| | | ±2.6 | ±0.17 | ±0.25 | ±0.017 | ±0.33 | ±0.43 | | ±0.10 |
| | Total | 169.2 | 8.67 | 25.24 | 0.187 | 49.63 | 59.83 | ≡100 | 26.24 |
| | | ±2.8 | ±0.14 | ±0.26 | ±0.013 | ±0.35 | ±0.46 | | ±0.11 |
| 72215,64 | 700 | 25.4 | 2.02 | 8.13 | 0.029 | 25.35 | 27.55 | ≡100 | 29.51 |
| (GCBx) | | ±0.8 | ±0.13 | ±0.17 | ±0.033 | ±0.23 | ±0.18 | | ±0.30 |
| | 1650 | 142.6 | 8.65 | 25.31 | 0.178 | 49.77 | 59.97 | ≡100 | 26.08 |
| | | ±4.4 | ±0.15 | ±0.18 | ±0.015 | ±0.24 | ±0.37 | | ±0.13 |
| | Total | 167.9 | 7.65 | 22.71 | 0.157 | 46.08 | 55.07 | ≡100 | 26.59 |
| | | ±4.5 | ±0.13 | ±0.19 | ±0.013 | ±0.25 | ±0.37 | | ±0.12 |
| 72215,92 | 700 | 24.9 | 2.54 | 9.51 | 0.017 | 27.84 | 31.09 | ≡100 | 28.93 |
| (GCBx) | | ±0.6 | ±0.10 | ±0.28 | ±0.025 | ±0.31 | ±0.49 | | ±0.41 |
| | 1650 | 114.6 | 12.60 | 34.60 | 0.286 | 62.94 | 77.86 | ≡100 | 24.62 |
| | | ±2.4 | ±0.15 | ±0.29 | ±0.012 | ±0.61 | ±0.48 | | ±0.15 |
| | Total | 139.5 | 10.81 | 30.12 | 0.238 | 56.68 | 69.51 | ≡100 | 25.39 |
| | | ±2.5 | ±0.13 | ±0.27 | ±0.011 | ±0.53 | ±0.46 | | ±0.14 |
| 72255,42 | 600 | 25 | 0.58 | 3.65 | 0.005 | 18.3 | 21.8 | ≡100 | 30.45 |
| (CN) | | ±11 | ±0.27 | ±0.42 | ±0.112 | ±1.3 | ±0.8 | | ±1.46 |
| | 1650 | 162 | 3.98 | 13.2 | 0.073 | 34.0 | 39.8 | ≡100 | 27.58 |
| | | ±28 | ±0.32 | ±1.3 | ±0.042 | ±1.7 | ±2.4 | | ±0.59 |
| | Total | 187 | 3.53 | 11.9 | 0.064 | 31.9 | 37.4 | ≡100 | 27.96 |
| | | ±30 | ±0.33 | ±1.2 | ±0.039 | ±1.7 | ±2.3 | | ±0.57 |
| 72255,52 | 600 | 33 | 0.88 | 6.52 | 0.000 | 21.52 | 21.52 | ≡100 | 30.54 |
| (GCBx) | | ± 4 | ±0.04 | ±0.31 | ±0.002 | ±0.22 | ±0.14 | | ±0.15 |
| | 1650 | 235 | 5.94 | 17.76 | 0.116 | 39.08 | 45.72 | ≡100 | 27.80 |
| | | ±29 | ±0.08 | ±0.21 | ±0.009 | ±0.34 | ±0.35 | | ±0.15 |
| | Total | 268 | 5.32 | 16.38 | 0.101 | 36.92 | 41.75 | ≡100 | 28.14 |
| | | ±29 | ±0.12 | ±0.29 | ±0.008 | ±0.45 | ±0.55 | | ±0.14 |
| 72275,57 | 600 | 15.4 | 1.61 | 16.43 | 0.023 | 24.73 | 25.14 | ≡100 | 29.47 |
| (LFBx) | | ±1.5 | ±0.13 | ±1.18 | ±0.038 | ±0.61 | ±0.77 | | ±0.21 |
| | 1100 | 55.7 | 20.96 | 52.11 | 0.336 | 78.28 | ≡100 | 66.5 | 11.43 |
| | | ±2.5 | ±0.29 | ±0.72 | ±0.014 | ±0.53 | | ±1.9 | ±0.41 |
| | 1650 | 23.9 | 19.50 | 50.14 | 0.335 | 79.00 | ≡100 | 77.3 | 15.28 |
| | | ±1.3 | ±0.26 | ±0.57 | ±0.022 | ±0.94 | | ±3.2 | ±0.96 |
| | Total | 95.1 | 23.95 | 63.5 | 0.390 | 99.1 | 1.251 | ≡100 | 19.80 |
| | | ±3.1 | ±0.67 | ±1.6 | ±0.018 | ±2.4 | ±0.033 | | ±0.27 |
| 72275,76 | 600 | 67 | 1.16 | 5.90 | 0.044 | 22.51 | 23.66 | ≡100 | 29.38 |
| (AnBx) | | ± 7 | ±0.07 | ±0.11 | ±0.032 | ±0.19 | ±0.31 | | ±0.46 |
| | 1650 | 320 | 7.70 | 23.33 | 0.133 | 46.89 | 55.31 | ≡100 | 27.04 |
| | | ±22 | ±0.22 | ±0.44 | ±0.018 | ±0.78 | ±0.94 | | ±0.26 |
| | Total | 387 | 6.57 | 20.31 | 0.117 | 42.67 | 49.83 | ≡100 | 27.45 |
| | | ±23 | ±0.22 | ±0.47 | ±0.016 | ±0.78 | ±0.96 | | ±0.23 |

*Table A.3 (Continued)*

| Sample | Temp. (°C) | $^{84}Kr$ ($10^{-12}$ cm$^3$ STP g$^{-1}$) | $^{78}Kr$ | $^{80}Kr$ | $^{81}Kr$ | $^{82}Kr$ | $^{83}Kr$ | $^{84}Kr$ | $^{86}Kr$ |
|---|---|---|---|---|---|---|---|---|---|
| 72275,80 | 600 | 71 | 0.90 | 5.32 | 0.090 | 21.79 | 21.94 | ≡100 | 28.47 |
| (BCBx) | | ±12 | ±0.14 | ±0.17 | ±0.054 | ±0.59 | ±0.50 | | ±1.46 |
| | 1650 | 429 | 7.76 | 23.60 | 0.120 | 45.4 | 52.4 | ≡100 | 27.46 |
| | | ±26 | ±0.28 | ±0.84 | ±0.020 | ±1.1 | ±1.4 | | ±0.29 |
| | Total | 500 | 6.79 | 21.01 | 0.116 | 42.0 | 48.1 | ≡100 | 27.60 |
| | | ±29 | ±0.29 | ±0.83 | ±0.019 | ±1.1 | ±1.4 | | ±0.32 |
| 72275,91 | Total | 139 | 9.6 | 34 | 0.144 | 63 | 76 | ≡100 | 25.9 |
| (PB) | | ±54 | ±3.2 | ±11 | ±0.073 | ±16 | ±22 | | ±1.9 |
| 72275,166 | 600 | 68 | 1.08 | 10.05 | 0.000 | 22.20 | 22.67 | ≡100 | 29.82 |
| (BCBx) | | ±10 | ±0.63 | ±0.30 | ±0.017 | ±0.25 | ±0.18 | | ±0.24 |
| | 1100 | 324 | 7.03 | 48.20 | 0.230 | 88.35 | ≡100 | 202.9 | 56.15 |
| | | ±49 | ±0.11 | ±0.45 | ±0.014 | ±0.59 | | ±1.3 | ±0.52 |
| | 1650 | 79 | 19.58 | 53.00 | 0.321 | 82.27 | ≡100 | 88.42 | 20.10 |
| | | ±12 | ±0.36 | ±0.54 | ±0.018 | ±0.54 | | ±0.22 | ±0.68 |
| | Total | 489 | 8.56 | 27.59 | 0.133 | 48.6 | 55.8 | ≡100 | 27.18 |
| | | ±51 | ±0.24 | ±0.70 | ±0.009 | ±1.4 | ±1.7 | | ±0.18 |

An additional uncertainty of ±10% in the absolute calibration should be applied to the abundance data.

TABLE A.4

Abundances and isotopic ratios of xenon in samples from Boulder 1, Station 2

| Sample | Temp. (°C) | $^{132}Xe$ ($10^{-12}$ cm$^3$ STP g$^{-1}$) | $^{124}Xe$ | $^{126}Xe$ | $^{128}Xe$ | $^{129}Xe$ | $^{130}Xe$ | $^{131}Xe$ | $^{134}Xe$ | $^{136}Xe$ |
|---|---|---|---|---|---|---|---|---|---|---|
| | | | $^{132}Xe \equiv 100$ | | | | | | | |
| 72215,60 | 700 | 7.3 | 0.70 | 0.90 | 7.96 | 98.75 | 15.84 | 81.5 | 39.35 | 33.12 |
| (GCBx) | | ±0.2 | ±0.06 | ±0.05 | ±0.18 | ±0.55 | ±0.27 | ±0.5 | ±0.34 | ±0.28 |
| | 1650 | 42.1 | 19.65 | 34.92 | 57.08 | 116.91 | 44.92 | 204.3 | 37.72 | 34.66 |
| | | ±0.9 | ±0.24 | ±0.27 | ±0.37 | ±0.33 | ±0.31 | ±0.6 | ±0.10 | ±0.25 |
| | Total | 49.4 | 16.86 | 29.90 | 49.84 | 114.24 | 40.63 | 186.2 | 37.96 | 34.44 |
| | | ±0.9 | ±0.22 | ±0.26 | ±0.37 | ±0.30 | ±0.29 | ±0.7 | ±0.10 | ±0.21 |
| 72215,64 | 700 | 6.4 | 0.77 | 0.95 | 7.51 | 97.10 | 15.07 | 79.7 | 38.91 | 33.53 |
| (GCBx) | | ±0.3 | ±0.07 | ±0.04 | ±0.19 | ±1.12 | ±0.34 | ±1.2 | ±0.36 | ±0.28 |
| | 1650 | 64.6 | 12.93 | 22.56 | 39.81 | 110.68 | 34.88 | 161.7 | 37.60 | 33.24 |
| | | ±2.9 | ±0.13 | ±0.20 | ±0.21 | ±0.29 | ±0.24 | ±0.6 | ±0.24 | ±0.17 |
| | Total | 71.0 | 11.84 | 20.62 | 36.91 | 109.46 | 33.10 | 154.4 | 37.72 | 33.26 |
| | | ±2.9 | ±0.13 | ±0.22 | ±0.26 | ±0.29 | ±0.25 | ±0.7 | ±0.22 | ±0.15 |
| 72215,92 | 700 | 2.9 | 1.43 | 2.30 | 9.54 | 99.07 | 16.14 | 86.1 | 38.86 | 34.26 |
| (GCBx) | | ±0.1 | ±0.15 | ±0.23 | ±0.31 | ±1.31 | ±0.71 | ±2.2 | ±0.24 | ±0.58 |
| | 1650 | 46.7 | 18.91 | 33.40 | 54.74 | 116.92 | 43.81 | 200.0 | 37.61 | 33.99 |
| | | ±1.1 | ±0.14 | ±0.18 | ±0.32 | ±0.37 | ±0.29 | ±0.7 | ±0.27 | ±0.19 |
| | Total | 49.5 | 17.90 | 31.60 | 52.13 | 115.89 | 42.21 | 193.4 | 37.68 | 34.01 |
| | | ±1.1 | ±0.14 | ±0.18 | ±0.32 | ±0.35 | ±0.29 | ±0.7 | ±0.26 | ±0.19 |
| 72255,42 | 600 | 6.8 | 0.38 | 0.47 | 7.67 | 95.45 | 14.25 | 79.3 | 38.40 | 32.29 |
| (CN) | | ±1.6 | ±0.15 | ±0.09 | ±0.43 | ±2.36 | ±0.63 | ±2.1 | ±1.36 | ±0.53 |
| | 1650 | 73.9 | 5.31 | 8.85 | 19.95 | 100.47 | 22.85 | 108.1 | 38.56 | 33.16 |
| | | ±4.8 | ±0.24 | ±0.47 | ±0.62 | ±0.69 | ±0.44 | ±1.4 | ±0.92 | ±0.33 |
| | Total | 80.7 | 4.90 | 8.15 | 18.92 | 100.05 | 22.12 | 105.6 | 38.54 | 33.08 |
| | | ±5.0 | ±0.24 | ±0.46 | ±0.61 | ±0.67 | ±0.44 | ±1.4 | ±0.85 | ±0.30 |
| 72255,52 | 600 | 7.0 | 0.31 | 0.63 | 7.55 | 99.83 | 15.54 | 79.5 | 38.95 | 33.23 |
| (GCBx) | | ±0.3 | ±0.07 | ±0.08 | ±0.14 | ±1.58 | ±0.13 | ±1.3 | ±0.52 | ±0.50 |
| | 1650 | 85.2 | 11.01 | 19.63 | 34.41 | 109.58 | 30.98 | 104.8 | 38.10 | 33.43 |
| | | ±2.6 | ±0.26 | ±0.30 | ±0.38 | ±0.84 | ±0.24 | ±0.9 | ±0.21 | ±0.22 |
| | Total | 92.2 | 10.19 | 18.18 | 32.36 | 108.83 | 29.80 | 136.1 | 38.16 | 33.41 |
| | | ±2.6 | ±0.25 | ±0.29 | ±0.36 | ±0.79 | ±0.22 | ±0.8 | ±0.20 | ±0.20 |

*Table A.4 (Continued)*

| Sample | Temp. (°C) | $^{132}Xe$ ($10^{-12}$ cm$^3$ STP g$^{-1}$) | $^{124}Xe$ | $^{126}Xe$ | $^{128}Xe$ | $^{129}Xe$ | $^{130}Xe$ | $^{131}Xe$ | $^{134}Xe$ | $^{136}Xe$ |
|---|---|---|---|---|---|---|---|---|---|---|
| | | | $^{132}Xe \equiv 100$ | | | | | | | |
| 72275,57 | 600 | 2.7 | 0.94 | 1.38 | 8.52 | 100.0 | 16.11 | 90.9 | 37.63 | 32.68 |
| (LFBx) | | ±0.1 | ±0.07 | ±0.12 | ±0.26 | ±1.1 | ±0.23 | ±0.7 | ±0.26 | ±0.45 |
| | 1100 | 31.7 | 36.42 | 61.48 | 94.12 | 147.1 | 61.86 | 308.0 | 29.87 | 25.64 |
| | | ±1.1 | ±0.43 | ±0.89 | ±0.77 | ±1.7 | ±0.49 | ±1.5 | ±0.17 | ±0.12 |
| | 1650 | 15.7 | 30.92 | 55.5 | 85.1 | 122.12 | 64.18 | 296.7 | 36.11 | 33.85 |
| | | ±0.6 | ±0.54 | ±1.0 | ±1.4 | ±0.65 | ±0.69 | ±2.5 | ±0.20 | ±0.19 |
| | Total | 50.1 | 32.75 | 56.31 | 86.62 | 136.7 | 60.09 | 292.6 | 32.25 | 28.60 |
| | | ±1.3 | ±0.34 | ±0.67 | ±0.70 | ±1.1 | ±0.40 | ±1.4 | ±0.15 | ±0.13 |
| 72275,76 | 600 | 16.1 | 0.55 | 0.52 | 7.14 | 94.99 | 15.01 | 80.0 | 39.59 | 32.76 |
| (AnBx) | | ±0.8 | ±0.04 | ±0.05 | ±0.27 | ±0.98 | ±0.21 | ±0.7 | ±0.56 | ±0.36 |
| | 1650 | 120.3 | 11.61 | 20.40 | 36.60 | 109.91 | 31.54 | 156.9 | 38.34 | 33.66 |
| | | ±3.8 | ±0.19 | ±0.47 | ±0.46 | ±0.76 | ±0.23 | ±1.1 | ±0.25 | ±0.23 |
| | Total | 136.4 | 10.30 | 18.05 | 33.12 | 108.15 | 29.59 | 147.8 | 38.48 | 33.55 |
| | | ±3.9 | ±0.18 | ±0.43 | ±0.44 | ±0.68 | ±0.22 | ±1.1 | ±0.23 | ±0.21 |
| 72275,80 | 600 | 22.6 | 0.58 | 0.71 | 7.67 | 97.4 | 15.03 | 80.7 | 38.57 | 33.45 |
| (BCBx) | | ±1.6 | ±0.05 | ±0.05 | ±0.29 | ±1.2 | ±0.48 | ±1.1 | ±0.50 | ±0.47 |
| | 1650 | 185.7 | 12.72 | 21.62 | 38.70 | 110.1 | 33.30 | 161.1 | 36.17 | 32.86 |
| | | ±7.2 | ±0.26 | ±0.59 | ±0.88 | ±2.1 | ±0.47 | ±3.7 | ±0.84 | ±0.28 |
| | Total | 208.3 | 11.40 | 19.36 | 35.34 | 108.7 | 31.32 | 152.4 | 36.43 | 32.93 |
| | | ±7.4 | ±0.26 | ±0.55 | ±0.83 | ±1.8 | ±0.45 | ±3.3 | ±0.75 | ±0.26 |
| 72275,91 | Total | 71.2 | 19.6 | 31.9 | 54.5 | 121.5 | 41.4 | 210 | 35.16 | 30.63 |
| (PB) | | ±9.6 | ±2.5 | ±4.2 | ±6.2 | ±3.2 | ±3.5 | ±17 | ±0.94 | ±0.43 |
| 72275,166 | 600 | 16.9 | 0.59 | 0.79 | 7.69 | 99.83 | 15.60 | 81.7 | 38.57 | 32.94 |
| (BCBx) | | ±0.6 | ±0.05 | ±0.02 | ±0.12 | ±0.75 | ±0.18 | ±0.5 | ±0.21 | ±0.18 |
| | 1100 | 149.2 | 9.61 | 16.27 | 30.03 | 107.40 | 28.69 | 144.5 | 36.80 | 31.74 |
| | | ±4.7 | ±0.14 | ±0.26 | ±0.33 | ±0.79 | ±0.22 | ±0.8 | ±0.16 | ±0.11 |
| | 1650 | 56.8 | 23.77 | 41.23 | 64.85 | 117.43 | 47.96 | 227.1 | 39.98 | 37.01 |
| | | ±1.8 | ±0.40 | ±0.65 | ±0.73 | ±0.89 | ±0.42 | ±1.8 | ±0.20 | ±0.02 |
| | Total | 222.9 | 12.53 | 21.46 | 37.21 | 109.38 | 32.61 | 160.8 | 37.75 | 33.17 |
| | | ±5.0 | ±0.18 | ±0.31 | ±0.40 | ±0.58 | ±0.24 | ±1.0 | ±0.13 | ±0.10 |

An additional uncertainty of ±10% in the absolute calibration should be applied to the abundance data.

## References


Alexander, E. C. and Davis, P. K.: 1974, *Geochim. Cosmochim. Acta* **38**, 911–928.

Alexander, E. C. and Kahl, S. B.: 1974, *Proc. Fifth Lunar Sci. Conf.* **2**, 1353–1373.

Alexander, E. C., Lewis, R. S., Reynolds, J. H., and Michel, M. C.: 1971, *Science* **172**, 837–840.

Banerjee, S. K. and Swits, G.: 1975, this issue, p. 473.

Blanchard, D. P., Haskin, L. A., Jacobs, J. W., Brannon, J. C., and Korotev. R. L.: 1974, *Interdisciplinary Studies of Samples from Boulder 1, Station 2, Apollo 17*, L.S.I. Contr. No. 211D, pp. IV-1–IV-15.

Blanchard, D. P., Haskin, L. A., Jacobs, J. W., Brannon, J. C., and Korotev, R. L.: 1975, this issue, p. 359.

Bogard, D. D., Funkhouser, J. G., Schaeffer, O. A., and Zahringer, J.: 1971, *J. Geophys. Res.* **76**, 2757–2779.

Browne, J. C. and Berman, B. L.: 1972, *Bull. Am. Phys. Soc.* **17**, 579.

Compston, W., Foster, J. J., and Gray, C. M.: 1975, this issue, p. 445.

Eberhardt, P., Geiss, J., Graf, H., Grögler, N., Krähenbuhl, U., Schwaller, H., and Stettler, A.: 1974, *Geochim. Cosmochim. Acta* **38**, 97–120.

Eberhardt, P., Geiss, J., Graf, H., Grögler, N., Mendia, M. D., Mörgeli, M., Schwaller, H., and Stettler, A.: 1972, *Proc. Third Lunar Sci. Conf.* **2**, 1821–1856.

Gast, P. W., Hubbard, N. J., and Wiesmann, H.: 1970, *Proc. Apollo 11 Lunar Sci. Conf.* **2**, 1143–1163.

Goswami, J. N. and Hutcheon, I. D.: 1975, this issue, p. 395.

Hintenberger, H., Weber, H. W., and Schultz, L.: 1974, *Proc. Fifth Lunar Sci. Conf.* **2**, 2005–2022.

Hohenberg, C. M., Davis, P. K., Kaiser, W. A., Lewis, R. S., and Reynolds, J. H.: 1970, *Proc. Apollo 11 Lunar Sci. Conf.* **2**, 1283–1309.

Huneke, J. C., Jessberger, E. K., Podosek, F. A., and Wasserburg, G. J.: 1973, *Proc. Fourth Lunar Sci. Conf.* **2**, 1725–1756.

Hutcheon, I. D. and Price, P. B.: 1972, *Science* **176**, 909–911.

Jessberger, E. K., Huneke, J. C., Podosek, F. A., and Wasserburg, G. J.: 1974, *Proc. Fifth Lunar Sci. Conf.* **2**, 1419–1449.

Leich, D. A. and Niemeyer, S.: 1975, *Proc. Sixth Lunar Sci. Conf.* **2**, (in press).

Leich, D. A., Kahl, S. B., Kirschbaum, A. R., Niemeyer, S., and Phinney, D.: 1974, *Interdisciplinary Studies of Samples from Boulder 1, Station 2, Apollo 17*, L.S.I. Contr. No. 211D, pp. VI-1–VI-18.

Lightner, B. D. and Marti, K.: 1974, *Proc. Fifth Lunar Sci. Conf.* **2**, 2023–2031.

Lingenfelter, R. E., Canfield, E. H., and Hampel, V. E.: 1972, *Earth Planetary Sci. Letters* **16**, 355–369.

Mark, R. K., Cliff, R. A., Lee-Hu, C., and Wetherill, G. W.: 1973, *Proc. Fourth Lunar Sci. Conf.* **2**, 1785–1795.

Marti, K.: 1967, *Phys. Rev. Letters* **18**, 264–266.

Marti, K. and Lugmair, G. W.: 1971, *Proc. Second Lunar Sci. Conf.* **2**, 1591–1605.

Marti, K., Lightner, B. D., and Lugmair, G. W.: 1973a, *Moon* **8**, 241–250.

Marti, K., Lightner, B. D., and Osborn, T. W.: 1973b, *Proc. Fourth Lunar Sci. Conf.* **2**, 2037–2048.

Marti, K., Lugmair, G. W., and Urey, H. C.: 1970, *Proc. Apollo 11 Lunar Sci. Conf.* **2**, 1357–1367.

Marvin, U. B.: 1974a, *Interdisciplinary Studies of Samples from Boulder 1, Station 2, Apollo 17*, L.S.I. Contr. No. 210D, pp. 9–33, 161–191.

Marvin, U. B.: 1974b, *Interdisciplinary Studies of Samples from Boulder 1, Station 2, Apollo 17*, L.S.I. Contr. No. 211D, pp. B-1–B-13.

Marvin, U. B.: 1975, this issue, p. 315.

Morgan, J. W., Higuchi, H., and Anders, E.: 1975, this issue, p. 373.

Nier, A. O.: 1950, *Phys. Rev.* **79**, 450–454.

Nunes, P. D. and Tatsumoto, M.: 1974, *Interdisciplinary Studies of Samples from Boulder 1, Station 2, Apollo 17*, L.S.I. Contr. No. 210D, 145–148.

Nunes, P. D. and Tatsumoto, M.: 1975, this issue, p. 463.

Pepin, R. O., Basford, J. R., Dragon, J. C., Coscio, M. R., Jr., and Murthy, V. R.: 1974, *Proc. Fifth Lunar Sci. Conf.* **2**, 2149–2184.

Phinney, D., Kahl, S. B., and Reynolds J. H.: 1975, *Proc. Sixth Lunar Sci. Conf.* **2**, (in press).

Podosek, F. A.: 1972, *Geochim. Cosmochim. Acta* **34**, 341–365.

Podosek, F. A. and Huneke, J. C.: 1971, *Earth Planetary Sci. Letters* **12**, 73–82.
Podosek, F. A., Huneke, J. C., Burnett, D. S., and Wasserburg, G. J.: 1971, *Earth Planetary Sci. Letters* **10**, 199–216.
Ryder, G., Stoeser, D. B., Marvin, U. B., Bower, J. F., and Wood, J. A.: 1975, this issue, p. 327.
Schaeffer, O. A. and Husain, L.: 1975, *Lunar Science VI*, 707–709.
Stettler, A., Eberhardt, P., Geiss, J., and Grögler, N.: 1974, *Earth Planetary Sci. Letters* **23**, 453–461.
Stettler, A., Eberhardt, P., Geiss, J., Grögler, N., and Guggisberg, S.: 1975, *Lunar Science VI*, 771–773.
Srinivasan, B.: 1973, *Proc. Fourth Lunar Sci. Conf.* **2**, 2033–2044.
Tatsumoto, M., Nunes, P. D., Knight, R. J., and Unruh, D. M.: 1974, *Lunar Science V*, 774–776.
Turner, G., Cadogan, P. H., and Younge, C. J.: 1973, *Proc. Fourth Lunar Sci. Conf.* **2**, 1889–1914.
Turner, G., Huneke, J. C., Podosek, F. A., and Wasserburg, G. J.: 1972, *Proc. Third Lunar Sci. Conf.* **2**, 1589–1612.
Wetherill, G. W.: 1953, *Phys. Rev.* **92**, 907–912.
Wood, J. A.: 1975, this issue, p. 505.
Wolfe, E. W.: 1975, this issue, p. 307.
Woolum, D. S. and Burnett, D. S.: 1974, *Earth Planetary Sci. Letters* **21**, 153–163.